IEEE Access
Multidisciplinary ⋮ Rapid Review ⋮ Open Access Journal

Received 20 May 2023, accepted 17 August 2023, date of publication 28 August 2023, date of current version 7 September 2023.

Digital Object Identifier 10.1109/ACCESS.2023.3309555

RESEARCH ARTICLE

Mixed Coded RF/FSO EH-Based Communication System Subject to Multiuser Interference and Residual Hardware Impairments

SOUAD LABGHOUGH[1], FOUAD AYOUB[2], (Member, IEEE), FAISSAL EL BOUANANI[1], (Senior Member, IEEE), MOSTAFA BELKASMI[1], (Member, IEEE), AND KHALID A. QARAQE[3], (Senior Member, IEEE)

[1]ENSIAS, Mohammed V University in Rabat, Rabat 10500, Morocco
[2]CRMEF, Kenitra 14026, Morocco
[3]Department of Electrical and Computer Engineering, Texas A&M University at Qatar, Ar-Rayyan, Qatar

Corresponding author: Khalid A. Qaraqe (khalid.qaraqe@qatar.tamu.edu)

This work was supported in part by the Qatar National Research Fund (a member of the Qatar Foundation) under Grant NPRP14C-0909-210008, and in part by the Qatar National Library.

ABSTRACT To increase spectral and power efficiencies, network coverage, and reduce outage probability, this study investigated the end-to-end performance of a coded dual-hop RF/FSO wireless communication system that operates across both Nakagami-m fading and Malaga-$\mathcal{M}$ atmospheric turbulence channels and is supplied with an amplify-and-forward semi-blind energy harvesting fixed-gain relay in order to increase spectral and power efficiencies, network coverage, and outage probability. We examine the use of CSOC codes at the source and a majority logic decoding method (MLGD) at the destination. Interestingly, our goal is to obtain an average bit error probability analytically by accounting for various interferers in the first hop as well as residual hardware impairments at the relay and destination receivers. As a consequence, the decoding method used in this investigation was shown to be adequate for the SWIPT/TS-assisted RF/FSO-coded AF cooperative communication system, requiring excellent accuracy while having a low computational cost.

INDEX TERMS Average bit error probability, energy harvesting, Málaga-$\mathcal{M}$ channels, maximal-ratio combining, mixed RF/FSO system, majority logic decoding, Nakagami-m fading channels, convolutional self orthogonal codes, residual hardware impairments.

I. INTRODUCTION

Intuitive networked communication environments are provided by fifth-generation (5G) mobile technology, connecting people, things, data, applications, transportation systems, and cities. The networks should be able to handle extraordinarily large volumes of data in record time, link a very large number of devices reliably, and transfer a significant amount of data more quickly. These lofty goals pose several difficulties for 5G networks. To handle more traffic and a faster data rate, the 5G network will need to use technology that is more spectrally efficient and has a substantially wider range of frequencies than the 3G and four-generation (4G) systems do [1].

Free space optical (FSO) communication requires a line of sight, high bandwidth, immunity to interference from other users' signals, ease of installation, and narrow beam width, which results in high physical layer security against potential listeners trying to overhear the lawful connection. To this end, FSO communication technology is the most appropriate technology to fulfill all the aforementioned requirements for a successful rollout of 5G, according to [2].

Despite all of the above benefits, there are still several barriers that hinder FSO from being widely used. Particularly, optical signals are substantially hampered by path-loss caused by atmospheric particles and molecules scattering [3]. Then, this scattering results in photon dispersion and

The associate editor coordinating the review of this manuscript and approving it for publication was Daniela Cristina Momete.

multipath fading [4]. Additionally, atmospheric turbulence and transceiver misalignment further reduce the average bit error probability's (ABEP) efficacy [5].

Importantly, it is crucial to provide an evolved strategy that combines both radio frequency (RF) and free space optical (FSO) links inside of a single platform due to the significant atmospheric limits placed upon FSO links. When the weather is clear, FSO links are often enabled to transfer the data, while RF links are employed when the atmosphere becomes less stable [6]. In this context, mixed dual-hop RF/FSO systems[1] have drawn the interest of many study areas because they combine the robustness of RF communications in difficult situations with both the cost-effectiveness and capabilities of FSO connections [7].

On the other hand, one of the primary aims of the forthcoming wireless communication systems (WCSs) (such as 5G and beyond, internet of things (IoT) [2]) is energy harvesting (EH), which has earned widespread attention as a potential means of developing self-sustaining and energy-efficient transmissions. It was recently suggested to use EH, which would allow the relaying node to collect wireless energy from the source and use it for re-transmission, to overcome the problem of a battery's short lifespan [8]. In particular, EH is viewed as a bright solution for IoT devices because one of these devices' main limitations is the finite battery capacity. This is because IoT devices consume a lot of energy when communicating with each other, limiting the amount of time that they can operate for as long as the battery lasts [9]. However, the majority of studies that evaluated the effectiveness of dual-hop EH-based WCS, including both [10], [11], are considered to be uncoded WCS.

Another crucial component of every WCS is security. Due to the variety of technologies and the amount of equipment connected to the system, it is a challenging process to do. To this purpose, all genuine WCS should include error-correcting codes in order to enhance physical layer security and boost efficiency [12], [13], [14], [15].

A. RELATED WORK

Numerous publications have evaluated the usefulness of uncoded WCSs while accounting for residual hardware impairments (RHI). For example, in [16], [17], [18], [19], and [20], the authors focused on the performance of uncoded WCS in single-hop or dual-hop configurations. Actually, in [21], the performance of a dual-hop mixed RF/FSO system with co-channel interference is explored for both fixed-gain and variable-gain amplify-and-forward (AF) relaying conditions. Furthermore, the authors of [22] investigate the performance of a cooperative network of unmanned aerial vehicles (UAVs) in which a source UAV sends data to a destination via intermediate relays using a 2-time slot transmission scheme, half duplexed (HD) transmission mode, and decode-and-forward (DF) protocol of relaying over Rayleigh fading channels using orthogonal frequency division multiple access (OFDMA).

Moreover, uncoded mixed RF/FSO performance under the effect of co-channel interference assumed at both relay and destination nodes [23] and asymmetric RF/FSO dual-hop cognitive amplify-and-forward (AF) relay networks affected by primary network interference [24] are among the studies investigating WCS efficiency under the effect of interference.

From another front, a few research studies, including [25], [26], [27], and [28] have explored the end-to-end (e2e) performance study of coded dual-hop WCS systems. For instance, using the Monte-Carlo simulation method, the authors in [29] and [30] studied the performance of low-density parity check (LDPC) codes over a hybrid FSO/RF parallel WCS and the evaluation of the polar codes across a few 5G scenarios, respectively. Additionally, hybrid FSO/RF communication systems can be improved using the EXIT Chart method, switching techniques and routing protocols as mentioned in [31] and [32]. Also, as studied in [33], the hybrid FSO/RF system outperforms the individual FSO and RF systems and gives a power gain of 3dB over a distinct number of receive antennas. Finally, performance analysis in [34] shows improved performance under strong turbulence, high pointing errors, and adverse weather conditions due to the RF backup link.

As previously stated, the bulk of research investigating the coded WCS are primarily focused with the simulation technique to assess efficiency [35], [30]. Additionally, the simulation script's execution period is crucial since the system must generate and manage a huge number of random samples. In order to address this major issue, the analytical representation for the metrics must be greatly reduced in order to considerably minimise the computing time necessary for ABEP evaluation purposes. To the best of our knowledge, no one has investigated the ABEP analysis of a mixed RF/FSO AF cooperative relaying system (i) employing error correcting codes, (ii) outfitted with energy harvesting, and (iii) taking interference into account.

B. MOTIVATION AND CONTRIBUTIONS

In light of the aforementioned explanation, we evaluate in this paper the ABEP performance of a coded dual-hop amplify-and-forward based RF/FSO system which is vulnerable to interference and RHI by taking into account convolutional self-orthogonal codes (CSOC) at the source and majority logic decoding (MLGD) at the destination. This later can efficiently decode CSOC codes with a higher number of memory registers in comparison with the Viterbi decoder, which is commonly used for convolutional codes with a short constraint length since its complexity rises with the number of encoder memory registers. Pointedly, the source node S in the system under study interacts with the destination node D through a relay node R. This latter amplifies the coded signal

[1] Mixed coded RF/FSO EH-based communication system, in which information is communicated between two terminals (nodes) via an EH-based relay, is regarded as a promising approach for increasing spectral and power efficiencies, network coverage, and reducing outage probability in infrastructure-less networks.

that was received from an RF fading channel and broadcasts it to D through an FSO channel. Specifically, the ABEP is presented in terms of the system and channel characteristics based on the cumulative distribution function (CDF) of the e2e signal-to-noise ratio (SNR). So, the methodology of this paper work is to first compute the end-to-end CDF of the entire uncoded transmission, for which we need to discover the distributions of SNRs of both RF and FSO connections while accounting for both scenarios of the energy harvesting process at the relay side. Then, the calculated e2e CDF is then used to produce the ABEP formulas for both uncoded and coded circumstances.

A basic description of this paper's main contributions is provided below:

- Under the assumption of EH' scenarios at the relay, Fox's H-function (FHF) is used to characterize the CDF of the e2e SNR.
- The ABEP expressions are then produced for the system under consideration's coded and uncoded scenarios.
- A significant decrease in the ABEP is produced in function of the number of antennas used at the relay, relay transmit power, the number of orthogonal equations, coding rate, RHI severity coefficient and pointing errors coefficient in order to get further insight into the performance of the proposed system.

C. ORGANIZATION

This article's remaining sections are organized as follows. Section II provides a description of the dual-hop system concept that is being suggested. Section III presents the e2e CDF computation in detail. For both coded and uncoded cases, Section IV presents the ABEP formulations. In Section V, the computational findings and instructive remarks are presented. Section VI, which also presents some suggestions for additional research, serves as the paper's final conclusion.

D. NOTATIONS

A list of the various notations used in this research is provided in Table 1.

II. SYSTEM AND CHANNEL MODEL

As shown in Fig. 1, the communication from S_1 to D through R is subject to the presence of interference and RHI at the relay and destination nodes. Thus, the received signal $r_i = \{r_{i,k}\}_{1\leq k\leq N_c}$ at the ith antenna of R during $(1-\varepsilon)T_1$ seconds is expressed as

$$r_{i,k} = \sqrt{L_1 P_{S_1}} h_{i,k}^{(S_1R)} x_k^{(1)} + \sum_{l=2}^{N_s} \sqrt{L_l P_{S_l}} h_{i,k}^{(S_lR)} x_k^{(l)} + v_{i,k}^{(R_r)} + n_{i,k};\ i = 1,\ldots,N_R, \tag{1}$$

where

- $L_l = G_{S_l} G_R \left(\frac{c}{4\pi d_0 f_l}\right)^2 \left(\frac{d_0}{d_{R_l}}\right)^\delta;\ l = 1,..,N_s$, where G_{S_l} and G_R are S and R's antennas gains, d_0 a reference distance, d_{R_l} denote the distance of the links $S_l - R$, c is the speed of light, f_l is the operating frequency, and δ is the path loss exponent,
- $v_{i,k}^{(R_r)}$ is the additive noise due to hardware impairment at R, with the variance $\sigma^2_{v_{R_r}} = R_c L_1 P_{S_1} (h_{i,k}^{(S_1R)})^2 \kappa^2_{v_{R_r}}$,
- $n_{i,k}$ is AWGN vector with zero-mean and variance $N = \sigma^2$.
- $h_{i,k}^{(S_lR)}$ as the complex fading coefficient vectors corresponding to the $S_l - R$ links, assumed independent and non-identically distributed (i.n.i.d) Nakagami-m random variables (RVs).
- N_R denotes the number of antennas at R,
- $x^{(l)} = \{x_k^{(l)}\}_{1\leq k\leq N_c, 1\leq l\leq N_s}$ as the modulated sequence, represented in the case of binary phase shift keying (BPSK) modulation as $x^{(l)} = 2c^{(l)} - 1$,
- N_c as the CSOC codeword length,
- $c^{(l)} = \{c_k^{(l)}\}_{1\leq k\leq N_c, 1\leq l\leq N_s}$ as the encoded data corresponding to the information sequence $d^{(l)}$,

Consequently, the corresponding instantaneous SINR of the $S_1 - R$ hop can be expressed as

$$\gamma_{i,k}^{(S_1R)} = \frac{\gamma_{i,k}^{(1)}}{\sum_{l=2}^{N_s} \gamma_{i.k}^{(l)} + \gamma_{i,k}^{(1)} \kappa^2_{v_{R_r}} + 1}, \tag{2}$$

where

$$\gamma_{i.k}^{(l)} = \frac{R_c L_l P_{S_l}}{N} \left| h_{i,k}^{(S_lR)} \right|^2, \tag{3}$$

being the instantaneous SNR for the ideal hardware scenario.

A. SNR OF S_1–R HOP

The received signals from S_1 are combined at the relay node using the MRC diversity combiner's N_R antennas. The overall SNR at the combiner's output can be evaluated as

$$\gamma_{S_1R} = \sum_{i=1}^{N_R} \gamma_i^{(S_1R)}. \tag{4}$$

For the sake of clarity, the index k will be removed in the variables in what follows. Specifically, $\gamma_{i,k}^{(S_1R)} = \gamma_i^{(S_1R)}$. The PDF/CDF of γ_{S_1R} can be tightly approximated by [36]

$$f_{\gamma_{S_1R}}(x) \approx a_1 G_{1,2}^{2,0}\left[\frac{x}{a_2}\middle| \begin{matrix} -; a_3 \\ a_4, a_5 \end{matrix}\right], \tag{5}$$

$$F_{\gamma_{S_1R}}(x) \approx a_1 x G_{2,3}^{2,1}\left[\frac{x}{a_2}\middle| \begin{matrix} 0; a_3 \\ a_4, a_5; -1 \end{matrix}\right], \tag{6}$$

where

$$a_1 = \frac{\Gamma(a_3+1)}{a_2 \Gamma(a_4+1)\Gamma(a_5+1)}, \tag{7}$$

$$a_3 = \frac{4\varphi_4 - 9\varphi_3 + 6\varphi_2 - \mu_1}{-\varphi_4 + 3\varphi_3 - 3\varphi_2 + \mu_1}, \tag{8}$$

$$a_2 = \frac{a_3}{2}(\varphi_4 - 2\varphi_3 + \varphi_2) + 2\varphi_4 - 3\varphi_3 + \varphi_2, \tag{9}$$

$$a_4 = \frac{a_6 + a_7}{2}, \tag{10}$$

$$a_5 = \frac{a_6 - a_7}{2}, \tag{11}$$

TABLE 1. List of functions and symbols.

Symbol	*Meaning*	*Symbol*	*Meaning*
r	Detection type	ε	Harvester efficiency
N_I	Source information length	T_1, T_2	First and second communication time
N_c	Coded signal length	P_{S_l}	S_l power
δ	Free space path-loss coefficient	G_0	Relay amplification gain
η	Power conversion efficiency	$F_X(.)$	CDF of the RV X
N_R	Number of antennas	$f_X(.)$	PDF of X
L_l	Path-loss parameter	$\lvert . \rvert$	Absolute value
d_{min}	Minimum distance	$\gamma_{inc}(.)$	Lower incomplete Gamma function
B_R	Battery capacity	$\mathbb{E}[.]$	Expectation operator
ξ	Pointing error parameter	$\Gamma(.)$	Gamma function
α, β	Málaga-$\mathcal{M}$ fading parameters	$G_{:,:}^{:,:}[.\lvert :]$	Meijer's G-function
n_c	CSOC encoder output bits	$H_{:,:,:,:,:}^{:,:,:,:,:}[.\lvert :]$	Bivariate FHF
K_i	Degree of a generator polynomial of a CSOC code	E_R	Harvested Energy
R_c	Coding rate	P_R	Harvested power
T	MLGD decoder correction capability	J	Number of orthogonal parity check-sums
m_c	CSOC encoder memory order	$m_i^{(l)}, \Omega_i^{(l)}$	Nakagami-m parameters
$\kappa_{v_{R_r}}$	RHI severity coefficient at R	$\kappa_{v_{D_r}}$	RHI severity coefficient at D
G_{S_l}	Source gain	d_{R_l}	$S_l - R$ distance
G_R	Relay gain	$\gamma_{S_1R}, \gamma_{RD}^{(\ell)}$	SNRs of the first and second hop, respectively
c	Speed of light	γ_{eq}	System's e2e SNR
d_0	Reference distance	f_l	The operating frequency
N_s	Number of interference sources		

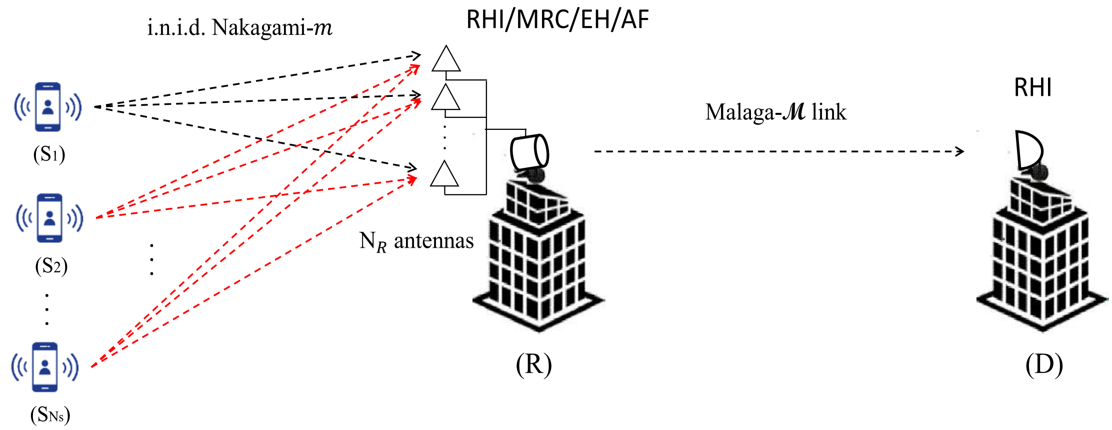

FIGURE 1. Communication system model.

$$a_6 = \frac{a_3(\varphi_2 - \mu_1) + 2\varphi_2 - \mu_1}{a_2} - 3, \tag{12}$$

$$a_7 = \sqrt{\left(\frac{a_3(\varphi_2 - \mu_1) + 2\varphi_2 - \mu_1}{a_2} - 1\right)^2 - 4\frac{\mu_1(a_3+1)}{a_2}}, \tag{13}$$

and

$$\varphi_i = \frac{\mu_i}{\mu_{i-1}}, i \geq 1, \tag{14}$$

where μ_i is the ith moment of the RV γ_{S_1R}, and $\Gamma(.)$ represents the Gamma function. Fig. 2 depicts the simulated and approximated PDF in (5) for different values of SNR.

B. SNR OF R–D HOP

Considering time switching (TS) protocol of EH, the energy harvested from the source S_1 and the interferers $S_2, \ldots, S_{N_s}$ during εT_1 seconds is given by

$$E_R = \theta \varepsilon T_1 \sum_{l=1}^{N_s} L_l P_{S_l} \sum_{i=1}^{N_R} \left| h_{i,k}^{(S_lR)} \right|^2, \tag{15}$$

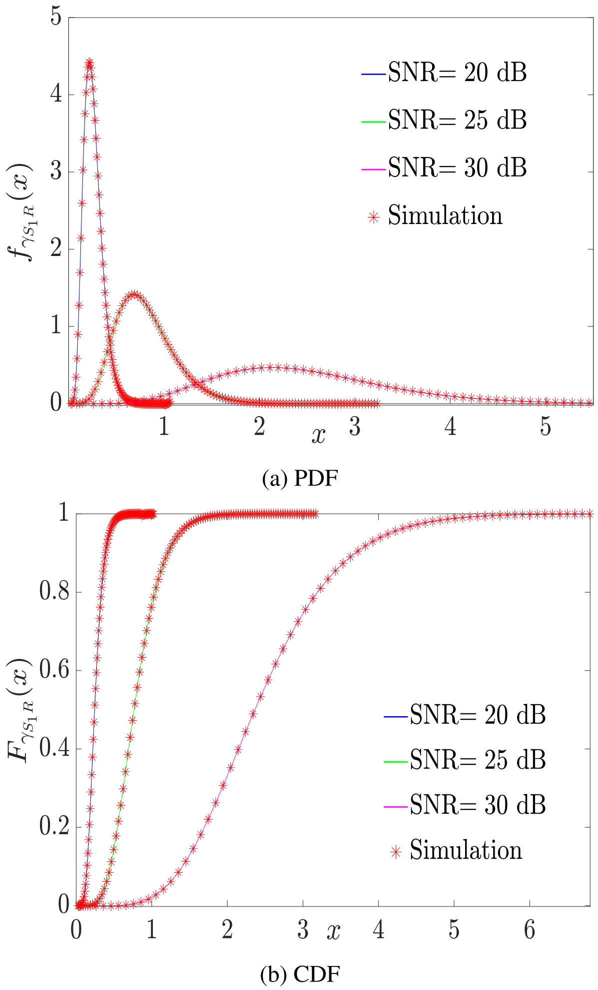

FIGURE 2. Approximated and simulated PDF/CDF of the sum of γ_{S_1R}.

where $0 < \varepsilon < 1$ and θ denoting the conversion efficiency of the energy harvester at the relay.

Throughout the second communication time T_2, the relay will use E_R to convey the signal to D. Given that the amount of energy gathered may be less or greater than the battery's capacity B_R. The transmit power is provided by $P_R = P_B = B_R/T_2$ if $E_R \geq B_R$, and $P_R = P_E = E_R/T_2$ otherwise. The PDF/CDF of P_E when $E_R < B_R$ can be accurately approximated by [37]

$$f_{P_R}(z) \approx \Psi^{m_I} \frac{z^{m_I-1}}{\Gamma(m_I)} \exp(-\Psi z), \tag{16}$$

$$F_{P_R}(z) \approx \frac{\gamma_{inc}(m_I, \Psi z)}{\Gamma(m_I)}, \tag{17}$$

where $\gamma_{inc}(.)$ represents lower incomplete Gamma function [38],

$$\Psi = \frac{\mathbb{E}[P_R]}{\mathbb{E}[P_R^2] - \mathbb{E}^2[P_R]}, \tag{18}$$

$$m_I = \frac{\mathbb{E}^2[P_R]}{\mathbb{E}[P_R^2] - \mathbb{E}^2[P_R]}, \tag{19}$$

$$\mathbb{E}[P_R] = \theta\varepsilon \frac{T_1}{T_2} \sum_{l=1}^{N_s} L_l P_{S_l} \sum_{i=1}^{N_R} \Omega_i^{(l)}, \tag{20}$$

and $\mathbb{E}[P_R^2]$ is written as in (21), shown at the bottom of the page, with $(l, i) \neq (l_0, i_0)$.

At D, the received information signal from R considering both heterodyne and IM/DD detection techniques can be written as

$$r_k^{(d)} = G_0 \sqrt{P_R} \left(\sqrt{\eta h_k^{(d)}}\right)^r r_k + v_k^{(D_r)} + n_k^{(d)}, \tag{22}$$

where

- $\sigma_{v_{D_r}}^2 = G_0^2 \left(\eta h_k^{(d)}\right)^r P_R \kappa_{v_{D_r}}^2$, as the variance of the additive noise $v_k^{(D_r)}$ due to hardware impairments at D,
- η denotes the photo-detector efficiency,
- $\{r_k\}_{1 \leq k \leq N_c}$ as the MRC combiner's output vector,
- $\{h_k^{(d)}\}_{1 \leq k \leq N_c}$ as the Málaga-$\mathcal{M}$ distributed light irradiance vector with the presence of pointing errors ξ [39], [40],
- $\{n_k^{(d)}\}_{1 \leq k \leq N_c}$ as AWGN vector with zero-mean and variance N_2,
- r represents the detection technique category (either IM/DD or heterodyne detection) and
- $G_0^2 = \frac{\mathbb{E}[P_R]}{NC}$ represents the fixed-gain semi-blind relaying where $C = \overline{\gamma}_{S_1R} + 1$ [41].

The corresponding SNR of the $R - D$ link can be obtained from (22) as

$$\gamma_{RD} = \frac{\gamma_{RD}^{(id)}}{\gamma_{RD}^{(id)} \kappa_{v_{D_r}}^2 + 1}, \tag{23}$$

where

$$\gamma_{RD}^{(id)} = P_R \gamma_2 = \frac{P_R \left(\eta h_k^{(d)}\right)^r}{N_2}. \tag{24}$$

By using (15), one obtains

$$\overline{\gamma}_{RD}^{(id)} = \begin{cases} \frac{m_I}{\Psi} \mu_r, E_R < B_R \\ P_B \mu_r, E_R \geq B_R, \end{cases} \tag{25}$$

$$\mathbb{E}[P_R^2] = \left(\theta\varepsilon \frac{T_1}{T_2}\right)^2 \left(\sum_{l=1}^{N_s} \sum_{i=1}^{N_R} \left(L_l P_{S_l}\right)^2 (m_i^{(l)} + 1)\Omega_i^{(l)} + \sum_{l=1}^{N_s} \sum_{i=1}^{N_R} L_l P_{S_l} \Omega_i^{(l)} \sum_{l_0=1}^{N_s} \sum_{i_0=1}^{N_R} L_{l_0} P_{S_{l_0}} \Omega_{i_0}^{(l_0)} \right), \tag{21}$$

where

$$\mu_r = \begin{cases} \overline{\gamma}, r = 1 \\ \frac{(\xi^2+2)(\xi^2+1)^{-2}\xi^2(\Omega'+g)^2}{(\alpha+1)\alpha^{-1}[\Omega'^2(1+\beta^{-1})+4\Omega' g+2g^2]}\overline{\gamma}, r = 2, \end{cases} \quad (26)$$

where $\overline{\gamma} = \frac{P_s}{N}$.

To characterize the statistical distribution of γ_{RD}, the distributions of RVs $P_R = P_E$ and γ_2 are required. The PDF for γ_2 is given as follows [42]

$$f_{\gamma_2}(\gamma_2) = \frac{\xi^2 A}{2r\gamma_2} \sum_{m_1=1}^{\beta} b_{m_1} G_{1,3}^{3,0}\left[B\left(\frac{\gamma_2}{\mu_r}\right)^{\frac{1}{r}} \middle| \begin{matrix} \xi^2+1 \\ \xi^2, \alpha, m_1 \end{matrix}\right], \quad (27)$$

while the PDF of P_R is being represented in (16).

Remark 1: It is worth mentioning that for the case of ideal hardware impairments, we have $\kappa^2_{v_{R_r}} = \kappa^2_{v_{D_r}} = 0$.

C. CSOC CODES AND MLGD DECODER

The coding method for a CSOC code with the coding rate $R_c = (n_c - 1)/n_c$ entails creating a parity symbol for each instant that corresponds to $(n_c - 1)$ information bits.

Essentially, the minimum distance $d_{min} = J + 1$ and a group of J equations describe these CSOC codes. Such codes are identified by the coding rate R_c and memory order m_c respectively, which are supplied by the formulas $R_c = (n_c - 1)/n_c$ and $m_c = \max_{1\leq i\leq n_c-1} K_i$, where K_i stands for the ith generator polynomial. Importantly, the input and output sequence lengths are indicated by $N_I \geq m_c + 1$ and $N_c = n_c(N_I + m_c)$, respectively. We denote the CSOC code using the syntax CSOC$(n_c, n_c - 1, m_c)$ for simplicity, [43], [44].

CSOC's MLGD decoding technique is what's known as an algebraic process. For the following reasons, this decoding method is different from Viterbi and sequential ones. Decoding techniques for Viterbi or sequential decoding are based on probabilistic, not algebraic, considerations. Furthermore, unlike Viterbi and sequential decoding methods, threshold decoding generates a final decision on the current information bit by simply taking into account the received coded symbols over a length $(m_c + 1)$, instead of considering the entire sequence of received coded symbols, [43], [44].

As a result, when D received the signal $r^{(d)}$, the MLGD decision is computed using straightforward logical operations with a correction capacity of $T = (d_{min} - 1)/2$ bits based on the set of J equations which are orthogonal each instant on the symbol under decoding [45].

Remark 2:

- *The studied MLGD decoder can adequately decode CSOC codes [46], in contrast to other decoding techniques as the Viterbi decoder, which is usually employed for convolutional codes with a low constraint length as its complexity grows with the memory order. Interestingly, the strong resistance to the encoded information that m_c may offer is its primary advantage; hence, the higher the m_c, the larger the coding gain and, consequently, the lower is the ABEP.*
- *Additionally, it is important to note that the greater the decoder's capacity to repair errant bits T is, the higher the number of orthogonal equationsÂ and minimum distance, and consequently,Â the more secure the transmission.*

III. STATISTICAL PROPERTIES

The analytical expressions for the PDF/CDF of the second hop's SNR and the CDF of the e2e SNR in the above-mentioned P_R cases are given in this section.

Given that the relay R employs a fixed-gain AF relaying mechanism, the e2e SNR received at D is represented as [41]

$$\gamma_{eq}^{(\ell)} = \frac{\gamma_{S_1R}\gamma_{RD}^{(\ell)}}{\gamma_{RD}^{(\ell)} + C}, \ell = 1, 2, \quad (28)$$

where $\ell = 1$ for the case of $E_R < B_R$ and $\ell = 2$ for $E_R \geq B_R$. By considering the two possible scenarios $E_R < B_R$ and $E_R \geq B_R$, the CDF of γ_{eq} may be derived as [42]

$$\begin{aligned} F_{\gamma_{eq}}(z) &= F_{\gamma_{eq}^{(1)}}(z) \Pr\left(P_R < \frac{B_R}{T_2}\right) \\ &\quad + F_{\gamma_{eq}^{(2)}}(z) \Pr\left(P_R \geq \frac{B_R}{T_2}\right) \\ &= \mathcal{D}F_{\gamma_{eq}^{(1)}}(z) + (1-\mathcal{D}) F_{\gamma_{eq}^{(2)}}(z), \end{aligned} \quad (29)$$

where $\mathcal{D}$ is expressed using (17) and [47, Eq. 06.06.26.0004.01] as

$$\mathcal{D} = \frac{1}{\Gamma(m_I)} G_{1,2}^{1,1}\left[\Psi\frac{B_R}{T_2} \middle| \begin{matrix} 1 \\ m_I, 0 \end{matrix}\right]. \quad (30)$$

In order to obtain the CDF expression of γ_{eq}, we have to compute first the SNR's PDF of the $R - D$ hop under the two circumstances of E_R stated in Section II.

Remark 3: It is worth noting from (28), that when $\gamma_{RD}^{(\ell)}$ tends to infinity, the e2e SNR $\gamma_{eq} \approx \gamma_{S_1R}$. As a result, at a fixed value of $\overline{\gamma}_{S_1R}$, the system's ABEP performance stabilizes.

A. PDF OF $\gamma_{RD}^{(id)}$

So, to compute the PDF of $\gamma_{RD}^{(id)}$, we have two cases:

1) FIRST CASE $E_R < B_R$

$\gamma_{RD_1}^{(id)}$ is the product of two RVs P_R and γ_2. Thus the PDF of $\gamma_{RD_1}^{(id)}$ is obtained as

$$f_{\gamma_{RD_1}^{(id)}}(z) = \int_0^\infty \frac{1}{x} f_{P_R}\left(\frac{z}{x}\right) f_{\gamma_2}(x)dx. \quad (31)$$

Proposition 1: The PDF of $\gamma_{RD_1}^{(id)}$ can be expressed as

$$f_{\gamma_{RD_1}^{(id)}}(z) = \frac{\mathcal{Q}_1}{z} \sum_{m_1=1}^{\beta} b_{m_1} r^{\alpha+m_1-2} \times G_{1,2r+2}^{2r+2,0}\left[\mathcal{B}_1 z \middle| \begin{matrix} \frac{\xi^2}{r}+1 \\ \kappa_1 \end{matrix}\right], \quad (32)$$

where $\kappa_1 = \frac{\xi^2}{r}, \frac{\alpha}{r}, \ldots, \frac{\alpha+r-1}{r}, \frac{m_1}{r}, \ldots, \frac{m_1+r-1}{r}, m_I + 1.$

$$\mathcal{B}_1 = \frac{B^r \Psi}{r^{2r} \mu_r}. \tag{33}$$

and

$$\mathcal{Q}_1 = \frac{\xi^2 A}{2\Gamma(m_I)(2\pi)^{r-1}}. \tag{34}$$

Proof: The proof is presented in Appendix A. ■

2) SECOND CASE $E_R \geq B_R$

$\gamma_{RD_2}^{(id)}$ is the RV γ_2 scaled by the constant P_B. Hence the PDF of $\gamma_{RD_2}^{(id)}$ is expressed as

$$f_{\gamma_{RD_2}^{(2)}}(z) = \frac{1}{P_B} f_{\gamma_2}\left(\frac{z}{P_B}\right). \tag{35}$$

Substituting (27) into (35), one gets

$$f_{\gamma_{RD_2}^{(id)}}(z) = \frac{\mathcal{Q}_2}{z} \sum_{m_1=1}^{\beta} b_{m_1} G_{1,3}^{3,0}\left[B\left(\frac{z}{P_B \mu_r}\right)^{\frac{1}{r}} \middle| \begin{matrix} \xi^2+1 \\ \xi^2, \alpha, m_1 \end{matrix} \right], \tag{36}$$

where

$$\mathcal{Q}_2 = \frac{\xi^2 A}{2r}. \tag{37}$$

B. CDF OF $\gamma_{RD}^{(id)}$

Proposition 2: The CDF of $\gamma_{RD}^{(id)}$ for the both cases $E_R < B_R$ and $E_R \geq B_R$ is represented respectively as

$$F_{\gamma_{RD_1}^{(id)}}(z) = \mathcal{Q}_1 \sum_{m_1=1}^{\beta} b_{m_1} r^{\alpha+m_1-2} G_{2,2r+3}^{2r+2,1}\left[\mathcal{B}_1 x \middle| \begin{matrix} 1, \frac{\xi^2}{r}+1 \\ \kappa_1, 0 \end{matrix} \right]. \tag{38}$$

and

$$F_{\gamma_{RD_2}^{(id)}}(z) = \mathcal{Q}_2 r \sum_{m_1=1}^{\beta} b_{m_1} G_{2,4}^{3,1}\left[\mathcal{B}_2 z^{\frac{1}{r}} \middle| \begin{matrix} 1, \xi^2+1 \\ \xi^2, \alpha, m_1, 0 \end{matrix} \right]. \tag{39}$$

where

$$\mathcal{B}_2 = B\left(\frac{1}{P_B \mu_r}\right)^{\frac{1}{r}}. \tag{40}$$

Proof: The proof is presented in Appendix B. ■

C. CDF OF γ_{RD}

One can easily deduce the CDF of γ_{RD} from the previous subsection as

$$F_{\gamma_{RD}^{(\ell)}}(z) = \begin{cases} F_{\gamma_{RD_\ell}^{(id)}}(z)\left(\frac{z}{1-z\kappa_{v_{D_r}}^2}\right); & z < \frac{1}{\kappa_{v_{D_r}}^2} \\ 1; & z \geq \frac{1}{\kappa_{v_{D_r}}^2} \end{cases} \tag{41}$$

Hence

1) FIRST CASE $E_R < B_R$

$$F_{\gamma_{RD}^{(1)}}(z) = \mathcal{Q}_1 \sum_{m_1=1}^{\beta} b_{m_1} r^{\alpha+m_1-2} \times G_{2,2r+3}^{2r+2,1}\left[\mathcal{B}_1 \frac{z}{(1-z\kappa_{v_{D_r}}^2)} \middle| \begin{matrix} 1, \frac{\xi^2}{r}+1 \\ \kappa_1, 0 \end{matrix} \right]. \tag{42}$$

2) SECOND CASE $E_R \geq B_R$

$$F_{\gamma_{RD}^{(2)}}(z) = \mathcal{Q}_2 r \sum_{m_1=1}^{\beta} b_{m_1} \times G_{2,4}^{3,1}\left[\mathcal{B}_2\left(\frac{z}{(1-z\kappa_{v_{D_r}}^2)}\right)^{\frac{1}{r}} \middle| \begin{matrix} 1, \xi^2+1 \\ \xi^2, \alpha, m_1, 0 \end{matrix} \right]. \tag{43}$$

D. PDF OF γ_{RD}

The PDF of γ_{RD} is computed as follows

$$f_{\gamma_{RD}^{(\ell)}}(z) = \frac{1}{(1-z\kappa_{v_{D_r}}^2)^2} \frac{\partial F_{\gamma_{RD(\ell)}^{(id)}}\left(\frac{z}{(1-z\kappa_{v_{D_r}}^2)}\right)}{\partial z}; z < \frac{1}{\kappa_{v_{D_r}}^2} \tag{44}$$

Hence, one obtains

1) FIRST CASE $E_R < B_R$

$$f_{\gamma_{RD}^{(1)}}(z) = \mathcal{Q}_1 \sum_{m_1=1}^{\beta} b_{m_1} r^{\alpha+m_1-2} \frac{1}{z(1-z\kappa_{v_{D_r}}^2)} \times G_{1,2r+2}^{2r+2,0}\left[\mathcal{B}_1 \frac{z}{(1-z\kappa_{v_{D_r}}^2)} \middle| \begin{matrix} \frac{\xi^2}{r}+1 \\ \kappa_1 \end{matrix} \right]. \tag{45}$$

2) SECOND CASE $E_R \geq B_R$

$$f_{\gamma_{RD}^{(2)}}(z) = \frac{1}{z(1-z\kappa_{v_{D_r}}^2)} \mathcal{Q}_2 \sum_{m_1=1}^{\beta} b_{m_1} \times G_{1,3}^{3,0}\left[\mathcal{B}_2\left(\frac{z}{(1-z\kappa_{v_{D_r}}^2)}\right)^{\frac{1}{r}} \middle| \begin{matrix} -, \xi^2+1 \\ \xi^2, \alpha, m_1, - \end{matrix} \right]. \tag{46}$$

E. CDF OF THE e2e SNR

The CDF of $\gamma_{eq}^{(\ell)}$ can be straightforwardly obtained using (28) as

$$F_{\gamma_{eq}^{(\ell)}}(z) = \int_0^\infty F_{\gamma_{SR}}\left(z\left(1+\frac{C}{x}\right)\right) f_{\gamma_{RD}^{(\ell)}}(x)dx. \tag{47}$$

1) FIRST SCENARIO

Proposition 3: The e2e SNR's CDF for the first scenario (i.e., $E_R < B_R$) can be approximated by (48), as shown at the bottom of the next page.

Proof: The proof is presented in Appendix C. ■

2) SECOND SCENARIO

Proposition 4: The e2e SNR's CDF for the second scenario (i.e., $E_R \geq B_R$) can be approximated by (49), as shown at the next page.

Proof: The proof is presented in Appendix A. ∎

IV. ABEP ANALYSIS

A. UNCODED COMMUNICATION (UC)

1) EXACT ANALYSIS

When no error-correcting code is used in the system, the ABEP can be evaluated as [48]

$$P_b^{(u)} = \frac{1}{2\mathcal{A}_1}\int_0^\infty \exp(-q\gamma)\gamma^{p-1}F_{\gamma_{eq}}(\gamma)d\gamma, \quad (50)$$

where p and q are two modulation-dependent parameters and

$$\mathcal{A}_1 = \frac{\Gamma(p)}{q^p}. \quad (51)$$

The ABEP in (50) can be formulated as

$$P_b^{(u)} = \frac{\mathcal{D}P_{b,1} + (1-\mathcal{D})P_{b,2}}{2\mathcal{A}_1}, \quad (52)$$

where $P_{b,1}$ and $P_{b,2}$ are evaluated in the next subsections.

- First Scenario

Proposition 5: $P_{b,1}$ can be tightly approximated by (53), as shown at the next page.

Proof: The proof is presented in Appendix E. ∎

- Second Scenario

Proposition 6: $P_{b,2}$ can be tightly approximated by (54), as shown at the next page.

Proof: The proof is presented in Appendix E. ∎

2) ASYMPTOTIC ANALYSIS

Proposition 7: In the high SNR regime (i.e., $P_s/N \to \infty$), the uncoded system's ABEP can be asymptotically expressed as in (55) and (56), shown at the next page, for the first and second scenario of EH, respectively, where $z = \frac{1}{qa_2} \to 0$ and

$$\Omega^{(1)} = \frac{\Gamma(-a_4+a_5)\Gamma(p+a_4)}{(1+a_4)\Gamma(-a_4+a_3)\Gamma(-a_4)}\Gamma(-s_2-a_4+1+k), \quad (57)$$

$$\Omega^{(2)} = \frac{\Gamma(-a_5+a_4)\Gamma(p+a_5)}{(1+a_5)\Gamma(-a_5+a_3)\Gamma(-a_5)}\Gamma(-s_2-a_5+1+k), \quad (58)$$

$$\Omega^{(3)} = \frac{\Gamma(s_2-1-k+a_4)\Gamma(s_2-1-k+a_5)\Gamma(p-s_2+1+k)}{(2-s_2+k)\Gamma(s_2-1-k+a_3)\Gamma(s_2+1+k)}, \quad (59)$$

$$p_0 = \arg\min_{j\leq 3}\xi_j, \quad (60)$$

$$\Omega_1^{(1)} = \Omega^{(1)}\Gamma(-a_4), \quad (61)$$

$$\Omega_1^{(2)} = \Omega^{(2)}\Gamma(-a_5), \quad (62)$$

$$p_1 = \arg\min_{j\leq 2}\xi_j, \quad (63)$$

$$\Omega_2^{(1)} = \frac{\Gamma(-a_4+a_5)\Gamma(p+a_4)}{(1+a_4)\Gamma(-a_4+a_3)\Gamma(-a_4)}\Gamma\left(-\frac{s_3}{r}-a_4+1+k_2\right), \quad (64)$$

$$\Omega_2^{(2)} = \frac{\Gamma(-a_5+a_4)\Gamma(p+a_5)}{(1+a_5)\Gamma(-a_5+a_3)\Gamma(-a_5)}\Gamma\left(-\frac{s_3}{r}-a_5+1+k_2\right), \quad (65)$$

$$\Omega_2^{(3)} = \frac{\Gamma(\frac{s_3}{r}-1-k_2+a_4)\Gamma(\frac{s_3}{r}-1-k_2+a_5)}{(2-\frac{s_3}{r}+k_2)\Gamma(\frac{s_3}{r}-1-k_2+a_3)\Gamma\left(\frac{s_3}{r}+1+k_2\right)} \times \Gamma(p-\frac{s_3}{r}+1+k_2), \quad (66)$$

$$p_2 = \arg\min_{j\leq 3}\xi'_j, \quad (67)$$

$$p_3 = \arg\min_{j\leq 2}\xi'_j, \quad (68)$$

$$F_{\gamma_{eq}^{(1)}}(z) \approx Ca_1\mathcal{Q}_1\sum_{m_1=1}^{\beta} b_{m_1}r^{\alpha+m_1-2}\sum_{k=0}^{\infty}\frac{(-1)^k}{k!}\left(C\kappa_{v_{D_r}}^2\right)^k \times H_{1,0;3,3;2,2r+4}^{0,1;2,1;2r+4,0}\left[\frac{z}{a_2}, C\mathcal{B}_1\left|\begin{matrix}(-k,-1,1):(0,1);(a_3,1),(0,1):\left(\frac{\xi^2}{r}+1,1\right),(-k,1)\\ -:(a_4,1),(a_5,1);(-1,1):(\kappa_1,1),(0,1),(-1-k,1)\end{matrix}\right.\right] + \frac{a_1\mathcal{Q}_1}{\kappa_{v_{D_r}}^2}\sum_{m_1=1}^{\beta}b_{m_1}r^{\alpha+m_1-2}G_{2,3}^{2,1}\left[\frac{z}{a_2}\left|\begin{matrix}0;a_3\\a_4,a_5;-1\end{matrix}\right.\right]G_{2,2r+3}^{2r+3,1}\left[\frac{\mathcal{B}_1}{\kappa_{v_{D_r}}^2}\left|\begin{matrix}0;\frac{\xi^2}{r}+1\\ \kappa_1,0\end{matrix}\right.\right]. \quad (48)$$

$$
\begin{aligned}
F_{\gamma_{eq}^{(2)}}(z) \approx\ & C a_1 \mathcal{Q}_2 \sum_{m_1=1}^{\beta} b_{m_1} \sum_{k_2=0}^{\infty} \frac{(-1)^{k_2}}{k_2!} \left(C \kappa_{v_{D_r}}^2\right)^{k_2} \\
& \times H_{1,0;3,3;2,5}^{0,1;2,1;5,0}\left[\frac{z}{a_2}, \mathcal{B}_2 C^{\frac{1}{r}} \middle| \begin{matrix} \left(-k,-1,\frac{1}{r}\right):(0,1);(a_3,1),(0,1):\left(\xi^2+1,1\right),\left(-k,\frac{1}{r}\right) \\ -:(a_4,1),(a_5,1);(-1,1):\left(\xi^2,1\right),(\alpha,1),(m_1,1),\left(0,\frac{1}{r}\right),\left(-1-k,\frac{1}{r}\right) \end{matrix}\right] \\
& + \frac{a_1 \mathcal{Q}_2}{\kappa_{v_{D_r}}^2} \sum_{m_1=1}^{\beta} b_{m_1} G_{2,3}^{2,1}\left[\frac{z}{a_2} \middle| \begin{matrix} 0;\ a_3 \\ a_4, a_5;\ -1 \end{matrix}\right] H_{2,2r+3}^{2r+3,1}\left[\frac{\mathcal{B}_2}{\left(\kappa_{v_{D_r}}^2\right)^{\frac{1}{r}}} \middle| \begin{matrix} \left(0,\frac{1}{r}\right);\left(\xi^2+1,1\right) \\ \left(\xi^2,1\right),(\alpha,1),(m_1,1),\left(0,\frac{1}{r}\right) \end{matrix}\right].
\end{aligned} \tag{49}
$$

$$
\begin{aligned}
P_{b,1} \approx\ & \frac{C a_1 \mathcal{Q}_1}{q^p} \sum_{m_1=1}^{\beta} b_{m_1} r^{\alpha+m_1-2} \sum_{k=0}^{\infty} \frac{(-1)^k}{k!} \left(C \kappa_{v_{D_r}}^2\right)^k \\
& \times H_{1,0;4,3;2,2r+4}^{0,1;2,2;2r+4,0}\left[\frac{1}{q a_2}, C\mathcal{B}_1 \middle| \begin{matrix} (-k,-1,1):(0,1),(1-p,1);(a_3,1),(0,1):\left(\frac{\xi^2}{r}+1,1\right),(-k,1) \\ -:(a_4,1),(a_5,1);(-1,1):(\kappa_1,1),(0,1),(-1-k,1) \end{matrix}\right] \\
& + \frac{a_1 \mathcal{Q}_1}{q^p \kappa_{v_{D_r}}^2} \sum_{m_1=1}^{\beta} b_{m_1} r^{\alpha+m_1-2} G_{3,3}^{2,2}\left[\frac{1}{q a_2} \middle| \begin{matrix} 0, 1-p;\ a_3 \\ a_4, a_5;\ -1 \end{matrix}\right] G_{2,2r+3}^{2r+3,1}\left[\frac{\mathcal{B}_1}{\kappa_{v_{D_r}}^2} \middle| \begin{matrix} 0;\ \frac{\xi^2}{r}+1 \\ \kappa_1, 0 \end{matrix}\right].
\end{aligned} \tag{53}
$$

$$
\begin{aligned}
P_{b,2} \approx\ & \frac{C a_1 \mathcal{Q}_2}{q^p} \sum_{m_1=1}^{\beta} b_{m_1} \sum_{k_2=0}^{\infty} \frac{(-1)^{k_2}}{k_2!} \left(C \kappa_{v_{D_r}}^2\right)^{k_2} \\
& \times H_{1,0;4,3;2,5}^{0,1;2,2;5,0}\left[\frac{1}{q a_2}, \mathcal{B}_2 C^{\frac{1}{r}} \middle| \begin{matrix} \left(-k,-1,\frac{1}{r}\right):(0,1),(1-p,1);(a_3,1),(0,1):\left(\xi^2+1,1\right),\left(-k,\frac{1}{r}\right) \\ -:(a_4,1),(a_5,1);(-1,1):\left(\xi^2,1\right),(\alpha,1),(m_1,1),\left(0,\frac{1}{r}\right),\left(-1-k,\frac{1}{r}\right) \end{matrix}\right] \\
& + \frac{a_1 \mathcal{Q}_2}{q^p \kappa_{v_{D_r}}^2} \sum_{m_1=1}^{\beta} b_{m_1} G_{3,3}^{2,2}\left[\frac{1}{q a_2} \middle| \begin{matrix} 0, 1-p;\ a_3 \\ a_4, a_5;\ -1 \end{matrix}\right] H_{2,2r+3}^{2r+3,1}\left[\frac{\mathcal{B}_2}{\left(\kappa_{v_{D_r}}^2\right)^{\frac{1}{r}}} \middle| \begin{matrix} \left(0,\frac{1}{r}\right);\left(\xi^2+1,1\right) \\ \left(\xi^2,1\right),(\alpha,1),(m_1,1),\left(0,\frac{1}{r}\right) \end{matrix}\right].
\end{aligned} \tag{54}
$$

$$
\begin{aligned}
P_{b,1} \sim\ & \frac{C a_1 \mathcal{Q}_1}{q^p} \sum_{m_1=1}^{\beta} b_{m_1} r^{\alpha+m_1-2} \sum_{k=0}^{\infty} \frac{(-1)^k}{k!} \left(C \kappa_{v_{D_r}}^2\right)^k \Omega^{(p_0)} z^{\xi_{p_0}} \frac{1}{2\pi j} \int_{\mathcal{C}_2} \mathcal{I}_2(s_2) ds_2 \\
& + \frac{a_1 \mathcal{Q}_1}{q^p \kappa_{v_{D_r}}^2} \sum_{m_1=1}^{\beta} b_{m_1} r^{\alpha+m_1-2} \frac{1}{2\pi j} \Omega_1^{(p_1)} z^{\xi_{p_1}} \frac{1}{2\pi j} \int_{\mathcal{C}_2} \mathcal{I}_4(s_2) ds_2.
\end{aligned} \tag{55}
$$

$$
\begin{aligned}
P_{b,2} \sim\ & \frac{C a_1 \mathcal{Q}_2}{q^p} \sum_{m_1=1}^{\beta} b_{m_1} \sum_{k_2=0}^{\infty} \frac{(-1)^{k_2}}{k_2!} \left(C \kappa_{v_{D_r}}^2\right)^{k_2} \Omega_2^{(p_2)} z^{\xi'_{p_2}} \frac{1}{2\pi j} \int_{\mathcal{C}_3} \mathcal{I}_5(s_3) ds_3 \\
& + \frac{a_1 \mathcal{Q}_2}{q^p \kappa_{v_{D_r}}^2} \sum_{m_1=1}^{\beta} b_{m_1} \Omega_3^{(p_3)} z^{\xi'_{p_3}} \frac{1}{2\pi j} \int_{\mathcal{C}_3} \mathcal{I}_6(s_3) ds_3.
\end{aligned} \tag{56}
$$

$$\Omega_3^{(1)} = \Omega_2^{(1)}\Gamma(-a_4), \quad (69)$$

$$\Omega_3^{(2)} = \Omega_2^{(2)}\Gamma(-a_5), \quad (70)$$

with $\xi_1 = a_4$, $\xi_2 = a_5$ *and* $\xi_3 = 1-s_2+k$, *and* $\xi_1' = a_4$, $\xi_2' = a_5$ *and* $\xi_3' = 1 - \frac{s_3}{r} + k$.

Proof: The proof is represented in Appendix F. ■

B. CODED COMMUNICATION (CC)

Based on the system model considered in the presented work, and using the error probability expression obtained for the uncoded case, the ABEP of the suggested decoding procedure while using CSOC codes is supplied by [49]

$$P_b^{(c)} = \left(1 - P_b^{(u)}\right) \sum_{k=T+1}^{J} \binom{J}{k} \mathcal{X}^{(k)} + P_b^{(u)} \sum_{k=J-T}^{J} \binom{J}{k} \mathcal{X}^{(k)}, \quad (71)$$

where

$$\mathcal{X}^{(k)} = \mathcal{P}^k (1-\mathcal{P})^{J-k}, \quad (72)$$

$$T = \begin{cases} J/2; J \text{ is even} \\ \frac{J+1}{2}; J \text{ is odd} \end{cases}, \quad (73)$$

with

$$\mathcal{P} = \frac{1 - \left(1 - 2P_b^{(u)}\right)^{\sigma_0}}{2}, \quad (74)$$

and

$$\sigma_0 = J(n-1). \quad (75)$$

V. NUMERICAL RESULTS

This section quantitatively depicts the computed ABEP formulas for MLGD over the investigated system. Table 2 shows the default values for the system parameters used to create the numerical results. It is clear that our analytical results correspond completely with the simulation results produced using Dev C/C++ 4.9.[2] It is essential to note also that we primarily used 3 CSOC codes with varying coding gains, $R_c = 1/2, 2/3$, and $4/5$, for simulation.

Fig. 3 depicts the ABEP performance of the system under study for both coded and uncoded circumstances as a function of the average SNR per symbol of the first hop for N_R ranging from 1 to 8. The ABEP decreases as the number of antenna branches increases. Also, regardless of the value of N_R, the RHI used in the system model created error floors, particularly in the uncoded scenario. For instance, the ABEP of the MLGD at SNR = 30 dB where $N_R = 4$ is approximately 10^{-5}. However, for the uncoded case, the ABEP stabilizes at 10^{-3} for SNR $\geq$ 30 dB.

[2]The source codes for the simulations can be find in the following link: https://github.com/1992LAB/BER_mixed_CSOC_RF_FSO_RHI_Journal2_1/tree/545c06914e819eae9d68023db190f3e7914130de

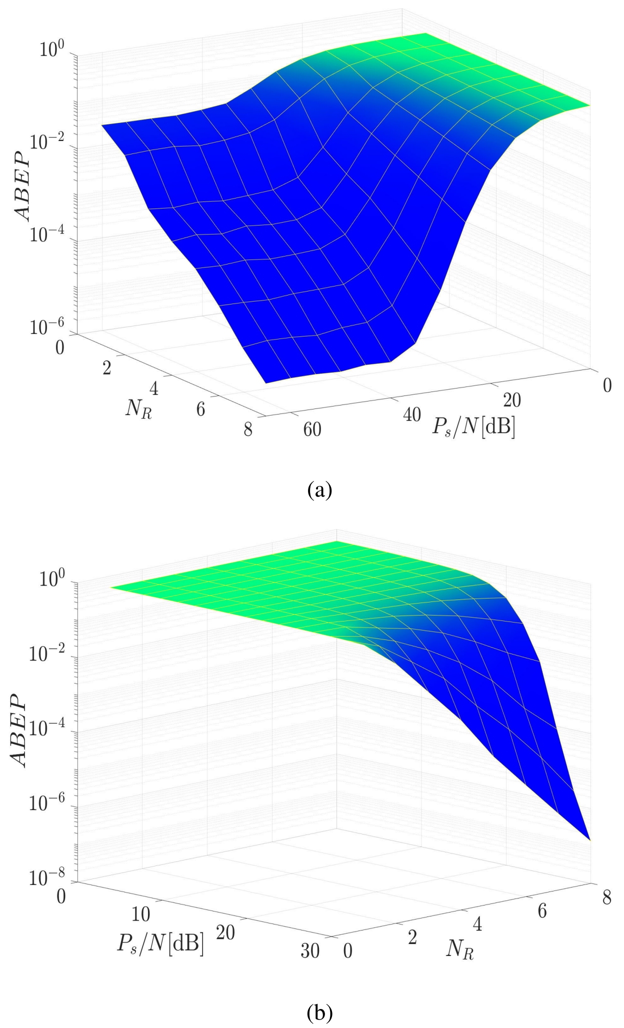

FIGURE 3. ABEP versus N_R for (a) uncoded and (b) coded communication CSOC(2,1,17).

TABLE 2. Simulation parameters.

Parameter	*Value*	*Parameter*	*Value*
ξ	6.7	α	8
β	4	d_0	100 m
η	0.9	ε	0.7
r	1	N_R	6
P_{S_1}	10 w	$T_1 = T_2$	1 s
θ	0.7	δ	2
d_{R_1}	60 m	B_R	500 mW
$d_{R_l}, l = 2, ..., N_s$	120 m	$P_{S_l}, l = 2, ..., N_s$	5 W
G_{S_1}	40 dB	$G_{S_l}, l = 2, ..., N_s$	10 dB
G_R	25 dB	N_s	3
c/f_l	28.6 mm dB	N_I	500 bits

In Fig. 4 (a), the ABEP performance is presented for various values of the RHI level of the destination receiver vs. P_s/N, where $N_R = 6$. One can plainly observe that when κ_{D_r} increases, the ABEP decreases substantially. Furthermore, the performance of the coded scenario utilising CSOC(5,4,26) outperforms the uncoded one, particularly in the region of small κ_{D_r} values.

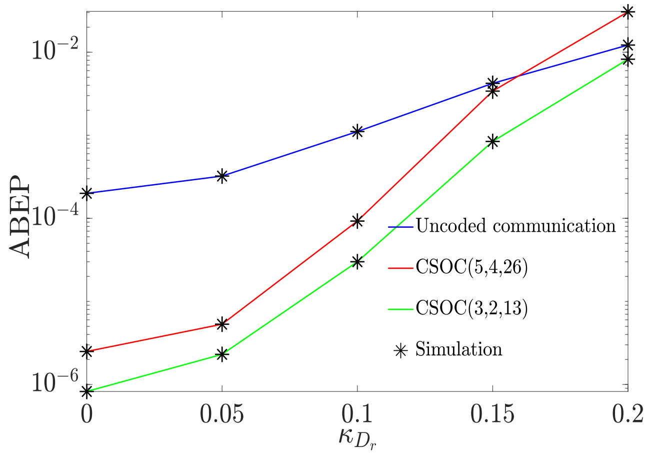

(a)

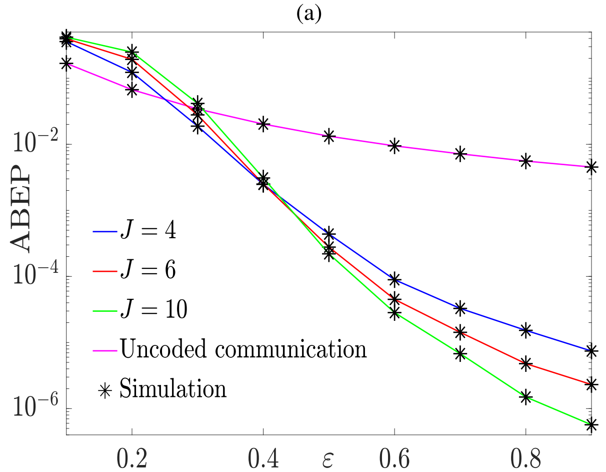

(b)

FIGURE 4. **(a) ABEP of the considered system vs RHI severity coefficient of the destination receiver. (b) ABEP vs ε.**

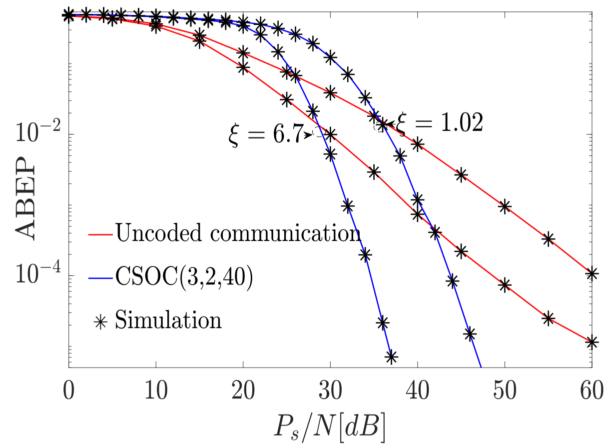

(a)

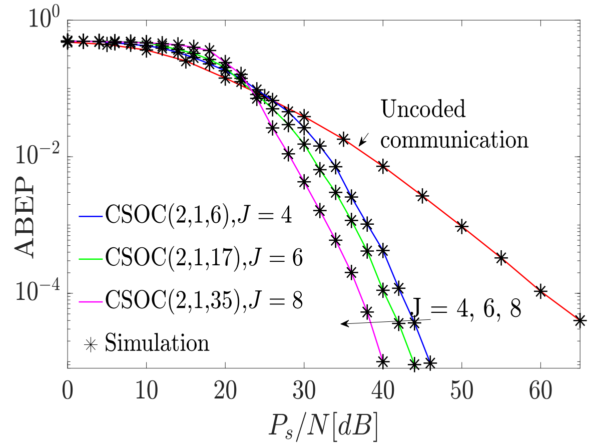

(b)

FIGURE 5. **(a) ABEP performance vs pointing error parameter. (b) ABEP performance vs the number of parity check sum equations J.**

Similar results are shown in Fig. 4 (b) for CSOC(3, 2, 13), CSOC(3, 2, 40) and CSOC(3, 2, 130). The ABEP is plotted in relation to the harvester efficiency ε. It is clear that when harvester efficiency improves, the ABEP decreases significantly. This indicates that when ε grows, so does the gathered power P_R, which permits the relay to deliver the information signal to D with more strength. Additionally, it is observable that there are a few points where the ABEP curves of coded and uncoded cases intersect. This problem arises mainly in the low SNRs area because of the large quantity of the recovered incorrect bits, which exceeds the decoder's correction capacity. However, after reaching a certain SNR' threshold while encountering turbulence of varying intensities, the ABEP performance of the coded system significantly increases.

For a variety of scenarios involving varying degrees of pointing error severity, the ABEP performance for the CSOC(3, 2, 40) code is displayed in Fig. 5 (a). It is worth noting that when ξ increases, the ABEP declines dramatically. It can be deduced that CSOC(3, 2, 40) earns approximately 15 dB at 10^{-4} when $\xi = 1.02$, and 13 dB when $\xi = 6.7$ at the same ABEP.

Fig. 5 (b) depicts the ABEP evolution for certain CSOC codes by examining various values of J under IM/DD detection. Remarkably, the higher orthogonal parity check sums number J improves the ABEP, confirming **Remark.** 2. One can observe that coding improvements of approximately 16 dB, 18 dB, and 20 dB are realized for $J = 4, 6$ and 8, respectively.

The ABEP performance of CSOC(2, 1, 55) is displayed in Fig. 6 by changing the d_{R_1} values. Concerningly, it is noticeable that when d_{R_1} increases, the ABEP increases dramatically. This indicates that the performance of the ABEP is impacted by the nodes' distance. Therefore, the system's overall performance degrades when the distance d_{R_1} grows up.

Interestingly, it is worth noting that the curves' behavior in the previous figures is well known in the literature for

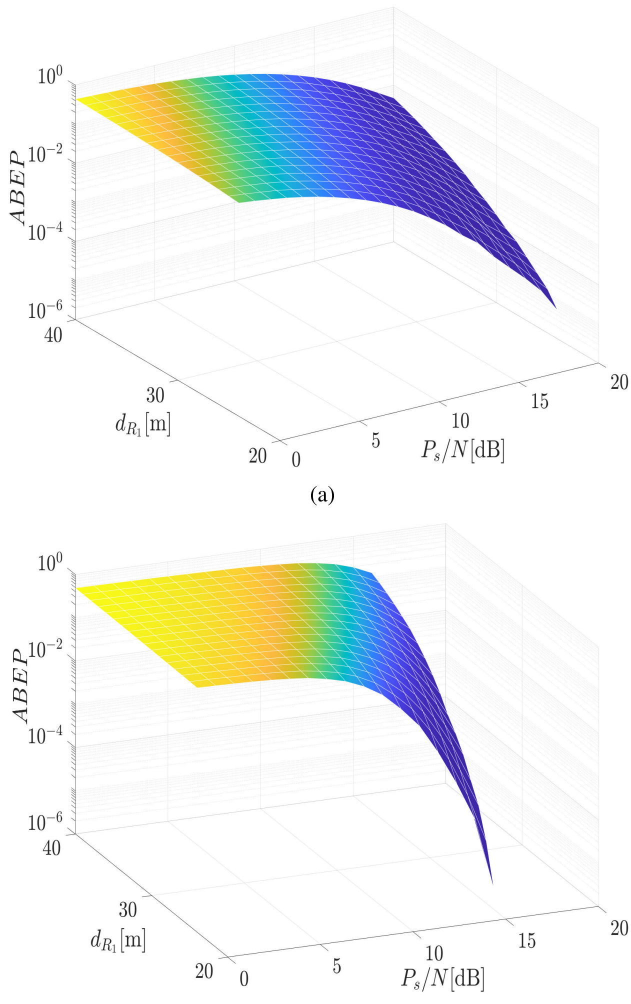

FIGURE 6. ABEP versus d_{R_1} for (a) uncoded and (b) coded communication CSOC(2,1,17).

coded WCS below a particular SNR threshold. In fact, this is due to the large number of erroneous bits recovered in the low SNR domain, which exceeds the decoder's capability for correction. The data is thus improperly decoded by the decoder in this SNR range. However, the number of erroneous bits rapidly drops when the SNR surpasses an SNR threshold and the coded communication performance improves.

Fig. 7 (a) depicts the ABEP performance as the number of interfering signals increases for both system model circumstances. Because we are receiving energy from the source S_1 and the $N_s - 1$ interferes, the figure shows that ABEP performance is about the same for all three N_s levels. Furthermore, error floors are significantly occurring as a result of the considered RHI at the relay and destination receivers, particularly in the uncoded situation.

The variation in ABEP for the two different kinds of detection techniques–IM/DD and heterodyne detection–is shown in Fig. 7 (b). From this figure, it is clearly seen that coherent demodulation ($r = 1$) outperforms better than receiver systems based on direct detection ($r = 2$).

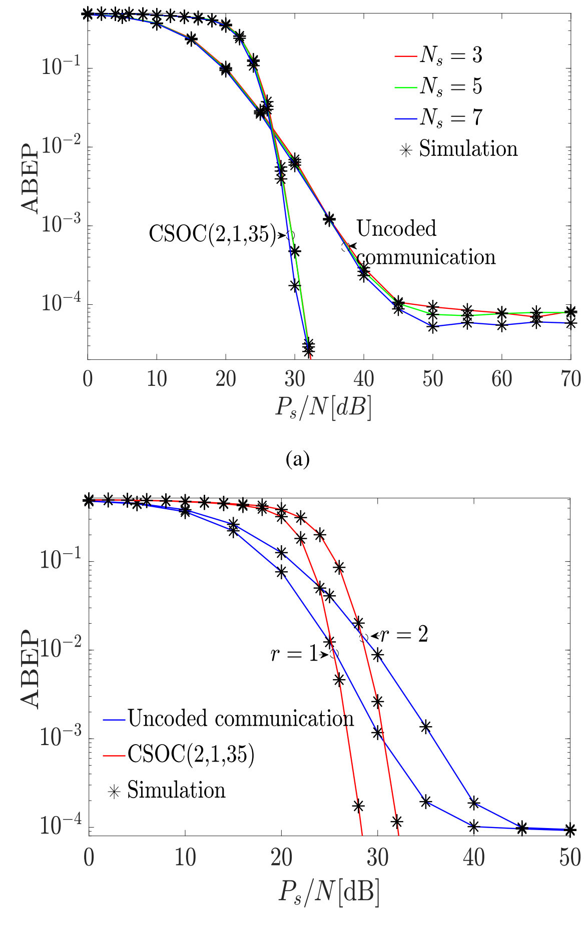

FIGURE 7. (a) ABEP vs P_S/N by varying the number of interferers effecting the system. (b) ABEP of the considered system vs r.

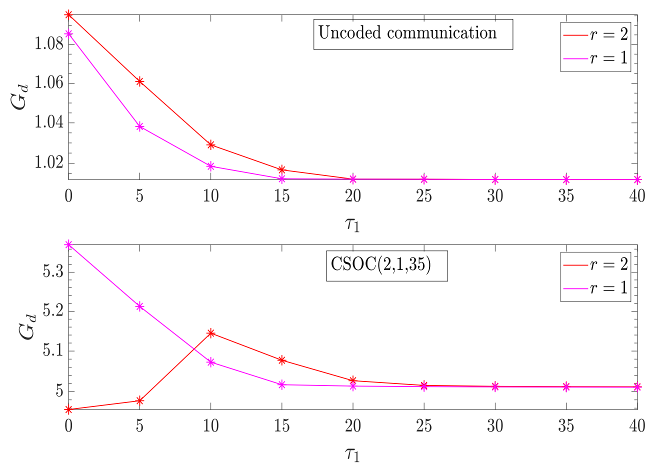

FIGURE 8. Diversity order for both heterodyne and IM/DD detection.

The diversity order of the system is depicted in Fig. 8, which was numerically assessed[3] and the ABEP curves of

[3]The diversity gain was numerically evaluated using the equation: $G_d \sim \frac{\log(P_{b_2}^{(u)})-\log(P_{b_1}^{(u)})}{\log(\tau_1)-\log(\tau_2)}$, where τ_i, $i = 1, 2$ are the average SNR values.

Fig. 7 (b), by adjusting the SNR τ_1 from 0 to 40 dB, while tau_2 remained constant. For example, the realised diversity order and coding gain of the uncoded scenario are $G_d \approx 1.01$ and $G_c \approx 0.03$, respectively, whereas $G_d \approx 5$ and $G_c \approx 0.0023$ for the coded case.

VI. CONCLUSION

In the presence of multiple interferes and RHI, the performance investigation of EH-based AF mixed coded RF/FSO dual-hop communication was examined. For both coded and uncoded cases, the analytical expression of the ABEP is derived specifically using the system's e2e CDF. Importantly, depending on how the system parameters were adjusted, the findings demonstrate that using the MLGD process for CSOC codes resulted in considerable coding improvements. Additionally, the number of relay antennas, $S_1 - R$ distance, relay transmit power, number of orthogonal equations, RHI severity, number of interferes, and pointing error impairments all affect the system's ABEP.

One novel idea that will be looked at in future studies is the performance analysis of satellite communication adopting polar coding. In addition, it is possible to analyze the performance of an RF/FSO dual-hop coded system while non-zero boresight pointing error for the FSO connection.

APPENDIX A
PROOF OF PROPOSITION 1

When $E_R < B_R$, the PDF of $\gamma_{RD_1}^{(id)}$ can be obtained by substituting (16) and (27) into (31) as

$$f_{\gamma_{RD_1}^{(id)}}(z) = z^{m_I-1}\frac{\Psi^{m_I}}{\Gamma(m_I)}\frac{\xi^2 A}{2r}\sum_{m_1=1}^{\beta} b_{m_1}\int_0^{\infty} x^{-m_I-1} \times G_{1,0}^{0,1}\left[\frac{x}{\Psi z}\middle| \begin{matrix}1\\ -\end{matrix}\right] G_{1,3}^{3,0}\left[B\left(\frac{x}{\mu_r}\right)^{\frac{1}{r}}\middle| \begin{matrix}\xi^2+1\\ \xi^2,\alpha,m_1\end{matrix}\right]dx. \tag{76}$$

By using [47, Eq. (01.03.26.0004.01)], [50, Eq. (6.2.2)] alongside [47, Eq. (07.34.21.0013.01)], (32) is obtained.

APPENDIX B
PROOF OF PROPOSITION 2

For the two cases $E_R < B_R$ and $E_R \geq B_R$, the CDF of $\gamma_{RD}^{(id)}$ is computed respectively as

A. FIRST CASE $E_R < B_R$

$$F_{\gamma_{RD_1}^{(id)}}(z) = \mathcal{Q}_1\sum_{m_1=1}^{\beta} b_{m_1} r^{\alpha+m_1-2}\mathcal{I}_1, \tag{77}$$

where

$$\mathcal{I}_1 = \int_0^z x^{-1} G_{1,2r+2}^{2r+2,0}\left[\mathcal{B}_1 x\middle| \begin{matrix}\frac{\xi^2}{r}+1\\ \kappa_1\end{matrix}\right]dx. \tag{78}$$

By using [47, Eq. (07.34.21.0003.01)], we can write $\mathcal{I}_1$ as

$$\mathcal{I}_1 = G_{2,2r+3}^{2r+2,1}\left[\mathcal{B}_1 x\middle| \begin{matrix}1,\frac{\xi^2}{r}+1\\ \kappa_1, 0\end{matrix}\right]. \tag{79}$$

Hence $F_{\gamma_{RD_1}^{(id)}}(z)$ is re-expressed as (38).

B. SECOND CASE $E_R \geq B_R$

In the same manner as the first case, $F_{\gamma_{RD_2}^{(id)}}(z)$ is expressed as

$$F_{\gamma_{RD_2}^{(id)}}(z) = \mathcal{Q}_2\sum_{m_1=1}^{\beta} b_{m_1}\int_0^z x^{-1} \times G_{1,3}^{3,0}\left[B\left(\frac{1}{P_B\mu_r}\right)^{\frac{1}{r}} x^{\frac{1}{r}}\middle| \begin{matrix}\xi^2+1\\ \xi^2,\alpha,m_1\end{matrix}\right]dx. \tag{80}$$

By making the change of variable $y = x^{\frac{1}{r}}$, (80) becomes

$$F_{\gamma_{RD_2}^{(id)}}(z) = \mathcal{Q}_2 r\sum_{m_1=1}^{\beta} b_{m_1}\int_0^{z^{\frac{1}{r}}} y^{-1} \times G_{1,3}^{3,0}\left[B\left(\frac{1}{P_B\mu_r}\right)^{\frac{1}{r}} y\middle| \begin{matrix}\xi^2+1\\ \xi^2,\alpha,m_1\end{matrix}\right]dy. \tag{81}$$

Then, by using [47, Eq. (07.34.21.0003.01)], we can write $F^{(2)}_{\gamma_{RD}^{(id)}}(z)$ as (39).

APPENDIX C
PROOF OF PROPOSITION 3

By substituting (6) and (32) into (47), one obtains

$$F_{\gamma_{eq}^{(1)}}(z) \approx \int_0^{\frac{1}{\kappa^2_{v_{D_r}}}} F_{\gamma_{S_1R}}\left(z\left(1+\frac{C}{x}\right)\right) f^{(1)}_{\gamma_{RD}}(x)dx \tag{82}$$

$$\approx a_1\mathcal{Q}_1\sum_{m_1=1}^{\beta} b_{m_1} r^{\alpha+m_1-2}\mathcal{I}_2(s_1,s_2), \tag{83}$$

where

$$\mathcal{I}_2(s_1,s_2) = \int_0^{\frac{1}{\kappa^2_{v_{D_r}}}} \frac{1}{(1-x\kappa^2_{v_{D_r}})} \times G_{2,3}^{2,1}\left[\left(\frac{z}{a_2}+\frac{z}{a_2}\frac{C}{x}\right)\middle| \begin{matrix}0; a_3\\ a_4,a_5;-1\end{matrix}\right] \times G_{1,2r+2}^{2r+2,0}\left[\mathcal{B}_1\frac{x}{(1-x\kappa^2_{v_{D_r}})}\middle| \begin{matrix}\frac{\xi^2}{r}+1\\ \kappa_1\end{matrix}\right]dx. \tag{84}$$

We have (85) and (86), as shown at the bottom of the next page, hence, $\mathcal{I}_2(s_1,s_2)$ becomes

$$\mathcal{I}_2(s_1,s_2) = \frac{1}{2\pi j}\int_{\mathcal{C}_1}\frac{\Gamma(s_1+a_4)\Gamma(s_1+a_5)\Gamma(1-s_1)}{\Gamma(s_1+a_3)\Gamma(2-s_1)} \times\left(\frac{z}{a_2}\right)^{-s_1}\frac{1}{2\pi j}\int_{\mathcal{C}_2}\frac{\Gamma(s_2+\frac{\xi^2}{r})}{\Gamma(s_2+\frac{\xi^2}{r}+1)}\mathcal{B}_1^{-s_2} \times\prod_{\ell=0}^{r-1}\Gamma\left(s_2+\frac{\alpha+\ell}{r}\right)\prod_{\ell=0}^{r-1}\Gamma\left(s_2+\frac{m_1+\ell}{r}\right) \times\Gamma(s_2+1+m_I)\mathcal{I}_3(s_1,s_2)ds_1 ds_2, \tag{87}$$

where

$$\mathcal{I}_3(s_1,s_2)=\left(\kappa_{v_{D_r}}^2\right)^{s_2-1}\int_0^{\frac{1}{\kappa_{v_{D_r}}^2}} x^{-s_2+s_1}(x+C)^{-s_1}\times\left(\frac{1}{\kappa_{v_{D_r}}^2}-x\right)^{s_2-1}dx. \tag{88}$$

By using [38, Eq. (3.197.8)], one obtains

$$\mathcal{I}_3(s_1,s_2)=\left(\kappa_{v_{D_r}}^2\right)^{s_2-1}\left(\frac{1}{C\kappa_{v_{D_r}}^2}\right)^{s_1}\frac{\Gamma(s_2)\Gamma(s_1-s_2+1)}{\Gamma(s_1+1)}\times{}_2F_1\left(s_1,s_1-s_2+1;s_1+1;-\frac{1}{C\kappa_{v_{D_r}}^2}\right), \tag{89}$$

with $Re(s_2-1)>0$, and $Re(s_1-s_2+1)>0$, where ${}_2F_1(.;.;.)$ denotes the Gauss hypergeometric function (GHF) [38]. Now, using the Mellin-Barnes integral representation of the GHF [38, Eq. (9.113)], it yields (90), as shown at the bottom of the page. Then, $\mathcal{I}_3(s_1,s_2)$ can be written as

$$\mathcal{I}_3(s_1,s_2)=\left(\kappa_{v_{D_r}}^2\right)^{s_2-1}\left(\frac{1}{C\kappa_{v_{D_r}}^2}\right)^{s_1}\frac{\Gamma(s_2)}{\Gamma(s_1)}\frac{1}{2\pi j}\int_{\mathcal{C}_t}\times\frac{\Gamma(s_1+t)\Gamma(s_1-s_2+1+t)\Gamma(-t)}{\Gamma(s_1+1+t)}\times\left(\frac{1}{C\kappa_{v_{D_r}}^2}\right)^t dt. \tag{91}$$

Hence, one gets

$$\mathcal{I}_2(s_1,s_2)=\frac{1}{2\pi j}\int_{\mathcal{C}_1}\frac{\Gamma(s_1+a_4)\Gamma(s_1+a_5)\Gamma(1-s_1)}{\Gamma(s_1+a_3)\Gamma(2-s_1)\Gamma(s_1)}\times\left(\frac{z}{a_2}\right)^{-s_1}\left(\frac{1}{C\kappa_{v_{D_r}}^2}\right)^{s_1}\frac{1}{2\pi j}\times\int_{\mathcal{C}_2}\frac{\Gamma(s_2+\frac{\xi^2}{r})\prod_{\ell=0}^{r-1}\Gamma\left(s_2+\frac{\alpha+\ell}{r}\right)}{\Gamma(s_2+\frac{\xi^2}{r}+1)}\times\prod_{\ell=0}^{r-1}\Gamma\left(s_2+\frac{m_1+\ell}{r}\right)\Gamma(s_2+1+m_I)\Gamma(s_2)\times\mathcal{B}_1^{-s_2}\left(\kappa_{v_{D_r}}^2\right)^{s_2-1}\mathcal{R}_1 ds_1 ds_2, \tag{92}$$

where

$$\mathcal{R}_1=\frac{1}{2\pi j}\int_{\mathcal{C}_t}\frac{\Gamma(s_1+t)\Gamma(s_1-s_2+1+t)\Gamma(-t)}{\Gamma(s_1+1+t)}\times\left(\frac{1}{C\kappa_{v_{D_r}}^2}\right)^t dt=\frac{1}{2\pi j}\int_{\mathcal{C}_t}\frac{\Gamma(s_1-s_2+1+t)\Gamma(-t)}{s_1+t}\left(\frac{1}{C\kappa_{v_{D_r}}^2}\right)^t dt. \tag{93}$$

As the conditions $\Delta=0$, [51, Eq. (1.1.8)], [52, Eq. (1.1.6)] and [52, Eq. (1.2.15)] are satisfied for the third Mellin Baren's integral, thus, by applying the residues theorem [52, Eq. (1.2)] on $\mathcal{R}_1$ it yields

$$\mathcal{R}_1\sim\sum_{k=0}^{\infty}\frac{(-1)^k}{k!}\frac{\Gamma(s_2-1-k)\Gamma(-s_2+s_1+1+k)}{\Gamma(s_2-k)}\times\left(C\kappa_{v_{D_r}}^2\right)^{-s_2+s_1+1+k}+\Gamma(1-s_2)\Gamma(s_1)\left(C\kappa_{v_{D_r}}^2\right)^{s_1}. \tag{94}$$

Consequently, substituting (94) into (92), (48) is attained in terms of bivariate FHF.

APPENDIX D
PROOF OF PROPOSITION 4

Likewise to $F_{\gamma_{eq}^{(1)}}(z)$, by replacing (6) and (36) in (47), one gets

$$F_{\gamma_{eq}^{(2)}}(z)\approx a_1\mathcal{Q}_2\sum_{m_1=1}^{\beta}b_{m_1}\mathcal{I}_4(s_1,s_3), \tag{95}$$

where

$$\mathcal{I}_4(s_1,s_3)=\int_0^{\frac{1}{\kappa_{v_{D_r}}^2}}\frac{1}{(1-x\kappa_{v_{D_r}}^2)}$$

$$G_{2,3}^{2,1}\left[\frac{z}{a_2}+\frac{z}{a_2}\frac{C}{x}\middle|\begin{matrix}0;a_3\\a_4,a_5;-1\end{matrix}\right]=\frac{1}{2\pi j}\int_{\mathcal{C}_1}\frac{\Gamma(s_1+a_4)\Gamma(s_1+a_5)\Gamma(1-s_1)}{\Gamma(s_1+a_3)\Gamma(2-s_1)}\left(\frac{z}{a_2}+\frac{z}{a_2}\frac{C}{x}\right)^{-s_1}ds_1. \tag{85}$$

$$G_{1,2r+2}^{2r+2,0}\left[\mathcal{B}_1\frac{x}{(1-x\kappa_{v_{D_r}}^2)}\middle|\begin{matrix}\frac{\xi^2}{r}+1\\\kappa_1\end{matrix}\right]=\frac{1}{2\pi j}\int_{\mathcal{C}_2}\frac{\Gamma(s_2+\frac{\xi^2}{r})\prod_{\ell=0}^{r-1}\Gamma\left(s_2+\frac{\alpha+\ell}{r}\right)\prod_{\ell=0}^{r-1}\Gamma\left(s_2+\frac{m_1+\ell}{r}\right)\Gamma(s_2+1+m_I)}{\Gamma(s_2+\frac{\xi^2}{r}+1)}\times\left(\mathcal{B}_1\frac{x}{(1-x\kappa_{v_{D_r}}^2)}\right)^{-s_2}ds_2. \tag{86}$$

$${}_2F_1\left(s_1,s_1-s_2+1;s_1+1;-\frac{1}{C\kappa_{v_{D_r}}^2}\right)=\frac{\Gamma(s_1+1)}{2\pi j\Gamma(s_1)\Gamma(s_1-s_2+1)}\int_{\mathcal{C}_t}\frac{\Gamma(s_1+t)\Gamma(s_1-s_2+1+t)\Gamma(-t)}{\Gamma(s_1+1+t)}\left(\frac{1}{C\kappa_{v_{D_r}}^2}\right)^t dt. \tag{90}$$

$$\times G_{2,3}^{2,1}\left[\frac{z\left(1+\frac{C}{x}\right)}{a_2}\middle|\begin{matrix}0; a_3\\ a_4, a_5; -1\end{matrix}\right]$$
$$\times G_{1,3}^{3,0}\left[\mathcal{B}_2\left(\frac{x}{(1-x\kappa_{v_{D_r}}^2)}\right)^{\frac{1}{r}}\middle|\begin{matrix}-, \xi^2+1\\ \xi^2, \alpha, m_1, -\end{matrix}\right]dx. \tag{96}$$

We have (97), as shown at the bottom of the page, so

$$\mathcal{I}_4(s_1,s_3)=\frac{1}{(2\pi j)^2}\int_{\mathcal{C}_1}\frac{\Gamma(s_1+a_4)\Gamma(s_1+a_5)\Gamma(1-s_1)}{\Gamma(s_1+a_3)\Gamma(2-s_1)}\times\left(\frac{z}{a_2}\right)^{-s_1}\int_{\mathcal{C}_3}\frac{\Gamma(s_3+\xi^2)\Gamma(s_3+\alpha)}{\Gamma(s_3+\xi^2+1)}\times\Gamma(s_3+m_1)\mathcal{B}_2^{-s_3}\mathcal{I}_5(s_1,s_3)ds_1ds_3, \tag{98}$$

where

$$\mathcal{I}_5(s_1,s_3)=\left(\kappa_{v_{D_r}}^2\right)^{\frac{s_3}{r}-1}\int_0^{\frac{1}{\kappa_{v_{D_r}}^2}}x^{s_1-\frac{s_3}{r}}(x+C)^{-s_1}\times\left(\frac{1}{\kappa_{v_{D_r}}^2}-x\right)^{\frac{s_3}{r}-1}dx. \tag{99}$$

By using [38, 3.197.8], one obtains

$$\mathcal{I}_5(s_1,s_3)=\left(\kappa_{v_{D_r}}^2\right)^{\frac{s_3}{r}-1}\left(C\kappa_{v_{D_r}}^2\right)^{-s_1}\times\frac{\Gamma\left(\frac{s_3}{r}\right)\Gamma\left(s_1-\frac{s_3}{r}+1\right)}{\Gamma(s_1+1)}\times{}_2F_1\left(s_1,s_1-\frac{s_3}{r}+1;s_1+1;-\frac{1}{C\kappa_{v_{D_r}}^2}\right), \tag{100}$$

where $Re(\frac{s_3}{r})>0$, and $Re(s_1-\frac{s_3}{r}+1)>0$. Now, using the Mellin-Barnes integral representation of the GHF [38, Eq. (9.113)], yields (101), as shown at the bottom of the page. Hence

$$\mathcal{I}_5(s_1,s_3)=\left(\kappa_{v_{D_r}}^2\right)^{\frac{s_3}{r}-1}\left(\frac{1}{C\kappa_{v_{D_r}}^2}\right)^{s_1}\frac{\Gamma\left(\frac{s_3}{r}\right)}{2\pi j\Gamma(s_1)}\times\int_{\mathcal{C}_v}\frac{\Gamma(s_1+v)\Gamma\left(s_1-\frac{s_3}{r}+1+v\right)\Gamma(-v)}{\Gamma(s_1+1+v)}\times\left(\frac{1}{C\kappa_{v_{D_r}}^2}\right)^{v}dv, \tag{102}$$

Then, one obtains

$$\mathcal{I}_4(s_1,s_3)=\frac{1}{2\pi j}\int_{\mathcal{C}_1}\frac{\Gamma(s_1+a_4)\Gamma(s_1+a_5)\Gamma(1-s_1)}{\Gamma(s_1+a_3)\Gamma(2-s_1)\Gamma(s_1)}\times\left(\frac{z}{a_2}\right)^{-s_1}\left(\frac{1}{C\kappa_{v_{D_r}}^2}\right)^{s_1}\frac{1}{2\pi j}\int_{\mathcal{C}_3}\times\frac{\Gamma(s_3+\xi^2)\Gamma(s_3+\alpha)\Gamma(s_3+m_1)\Gamma\left(\frac{s_3}{r}\right)}{\Gamma(s_3+\xi^2+1)}\times\mathcal{B}_2^{-s_3}\left(\kappa_{v_{D_r}}^2\right)^{\frac{s_3}{r}-1}\mathcal{R}_2ds_1ds_3. \tag{103}$$

where

$$\mathcal{R}_2=\frac{1}{2\pi j}\int_{\mathcal{C}_v}\frac{\Gamma\left(s_1-\frac{s_3}{r}+1+v\right)\Gamma(-v)}{s_1+v}\left(\frac{1}{C\kappa_{v_{D_r}}^2}\right)^{v}dv. \tag{104}$$

Similarly as the CDF of the first scenario, by applying the residues theorem [52, Eq. (1.2)], one obtains

$$\mathcal{R}_2\sim\sum_{k_2=0}^{\infty}\frac{(-1)^{k_2}}{k_2!}\frac{\Gamma\left(\frac{s_3}{r}-1-k\right)\Gamma\left(-\frac{s_3}{r}+s_1+1+k_2\right)}{\Gamma\left(\frac{s_3}{r}-k\right)}\times\left(C\kappa_{v_{D_r}}^2\right)^{-\frac{s_3}{r}+s_1+1+k_2}+\Gamma\left(1-\frac{s_3}{r}\right)\Gamma(s_1)\left(C\kappa_{v_{D_r}}^2\right)^{s_1}. \tag{105}$$

Consequently, by substituting (105) into (103), (49) is attained.

APPENDIX E
PROOF OF PROPOSITION 5

$P_{b,\ell}$ is written as follows

$$P_{b,\ell}\approx\int_0^{\infty}\gamma^{p-1}\exp(-q\gamma)F_{\gamma_{eq}^{(\ell)}}(\gamma)d\gamma. \tag{106}$$

where $P_{b,1}$ and $P_{b,2}$ are computed below.

1) $P_{b,1}$ EXPRESSION

Replacing (48) into (106) gives (107), as shown at the bottom of the next page, where

$$\mathcal{I}_6(s_1)=\int_0^{\infty}e^{-q\gamma}\gamma^{p-1-s_1}d\gamma=\Gamma(p-s_1)q^{-p+s_1}, \tag{108}$$

using [47, Eq. (07.34.21.0009.01)].

$$G_{1,3}^{3,0}\left[\mathcal{B}_2\left(\frac{x}{(1-x\kappa_{v_{D_r}}^2)}\right)^{\frac{1}{r}}\middle|\begin{matrix}-, \xi^2+1\\ \xi^2, \alpha, m_1, -\end{matrix}\right]=\frac{1}{2\pi j}\int_{\mathcal{C}_3}\frac{\Gamma(s_3+\xi^2)\Gamma(s_3+\alpha)\Gamma(s_3+m_1)}{\Gamma(s_3+\xi^2+1)}\left(\mathcal{B}_2\left(\frac{x}{(1-x\kappa_{v_{D_r}}^2)}\right)^{\frac{1}{r}}\right)^{-s_3}ds_3. \tag{97}$$

$${}_2F_1\left(s_1,s_1-\frac{s_3}{r}+1;s_1+1;-\frac{1}{C\kappa_{v_{D_r}}^2}\right)=\frac{\Gamma(s_1+1)}{2\pi j\Gamma(s_1)\Gamma\left(s_1-\frac{s_3}{r}+1\right)}\int_{\mathcal{C}_v}\frac{\Gamma(s_1+v)\Gamma\left(s_1-\frac{s_3}{r}+1+v\right)\Gamma(-v)}{\Gamma(s_1+1+v)}\times\left(C\kappa_{v_{D_r}}^2\right)^{-v}dv. \tag{101}$$

By replacing (108) into (107), together with the use of [53], (53), is attained in terms of bivariate FHF [47].

2) $P_{b,2}$ EXPRESSION

Equivalently as finding (53), (54) is derived using bivariate FHF [47].

APPENDIX F
PROOF OF PROPOSITION 6

A. FIRST SCENARIO

$P_{b,1}$ defined in (53), can be written as a Mellin-Barnes integral as (109), shown at the bottom of the page, where

$$\mathcal{I}_1(s_1) = \frac{\Gamma(s_1+a_4)\Gamma(s_1+a_5)\Gamma(1-s_1)\Gamma(p-s_1)}{\Gamma(s_1+a_3)\Gamma(2-s_1)\Gamma(s_1)}(qa_2)^{s_1}, \tag{110}$$

$$\mathcal{I}_2(s_2) = \frac{\Gamma(s_2+\frac{\xi^2}{r})\Gamma(s_2)\Gamma(s_2-1-k)}{\Gamma(s_2+\frac{\xi^2}{r}+1)\Gamma(s_2-k)} \times \prod_{\ell=0}^{r-1}\Gamma\left(s_2+\frac{\alpha+\ell}{r}\right)\prod_{\ell=0}^{r-1}\Gamma\left(s_2+\frac{m_1+\ell}{r}\right) \times \Gamma(s_2+1+m_I)(C\mathcal{B}_1)^{-s_2}, \tag{111}$$

$$\mathcal{I}_3(s_1) = \frac{\Gamma(s_1+a_4)\Gamma(s_1+a_5)\Gamma(1-s_1)\Gamma(p-s_1)}{\Gamma(s_1+a_3)\Gamma(2-s_1)}(qa_2)^{s_1}, \tag{112}$$

As the conditions $\Delta_0 = 0$ and $\delta = 1$ [51, Eqs. (1.1.8) and (1.1.9)] are satisfied, taking into account that s_2 is constant, in addition to $0 < z < 1$ where $z = \frac{1}{qa_2}$, the first part of $P_{b,1}$ can be written as infinite summation of residues evaluated at the left poles of $\mathcal{I}_1(s_1)$. Moreover, as we are interested in the asymptotic SNR (i.e., $z \to 0$), it is sufficient to evaluate the residue corresponding to the top left poles. i.e., only for the elements $a_4, a_4, 1+k-s_2$.

It's worth noting that $\mathcal{I}_1(s_1)$ admits only first-order (FO) LPs. Leveraging [51, Theorems 1.2, 1.4], their respective residues may be evaluated.

So, the residues of $\mathcal{I}_1(s_1)$ at a_4, a_4 and $1+k-s_2$ can be expressed, respectively as

$$\mathcal{T}^{(1)} \sim \Omega^{(1)} z^{a_4}, \tag{114}$$

$$\mathcal{T}^{(2)} \sim \Omega^{(2)} z^{a_5}, \tag{115}$$

$$\mathcal{T}^{(3)} \sim \Omega^{(3)} z^{-(s_2-1-k)}, \tag{116}$$

where $\Omega^{(1)}$, $\Omega^{(2)}$ and $\Omega^{(3)}$ are given by (57), (58) and (59).

For the second part of $P_{b,1}$, the condition $\Delta_0 = 0$ is satisfied for the first Meijer function, in addition to $0 < z = \frac{1}{qa_2} < \delta = 1$ [51, Eqs. (1.1.8) and (1.1.9)]. Consequently, the residues of $\mathcal{I}_3(s_1)$ can be expressed respectively as

$$\mathcal{T}_1^{(1)} = \mathcal{T}^{(1)}\Gamma(-a_4), \tag{117}$$

and

$$\mathcal{T}_1^{(2)} = \mathcal{T}^{(2)}\Gamma(-a_5). \tag{118}$$

Thus, the asymptotic expression for $P_{b,1}$ is obtained as (55).

B. SECOND SCENARIO

Similarly, as the first scenario, (56) is obtained for the second scenario.

$$P_{b,1} \approx Ca_1\mathcal{Q}_1\sum_{m_1=1}^{\beta} b_{m_1} r^{\alpha+m_1-2}\sum_{k=0}^{\infty}\frac{(-1)^k}{k!}\left(C\kappa_{v_{D_r}}^2\right)^k\frac{1}{2\pi j}\int_{\mathcal{C}_1}\frac{\Gamma(s_1+a_4)\Gamma(s_1+a_5)\Gamma(1-s_1)}{\Gamma(s_1+a_3)\Gamma(2-s_1)\Gamma(s_1)}\left(\frac{1}{a_2}\right)^{-s_1} \times \frac{1}{2\pi j}\int_{\mathcal{C}_2}\frac{\Gamma(s_2+\kappa_1)\Gamma(s_2)\Gamma(s_2-1-k)}{\Gamma(s_2+\frac{\xi^2}{r}+1)\Gamma(s_2-k)}(C\mathcal{B}_1)^{-s_2}\Gamma(-s_2+s_1+1+k)\mathcal{I}_6(s_1)ds_1ds_2 + \frac{a_1\mathcal{Q}_1}{\kappa_{v_{D_r}}^2}\sum_{m_1=1}^{\beta} b_{m_1} r^{\alpha+m_1-2}\frac{1}{2\pi j}\int_{\mathcal{C}_1}\frac{\Gamma(s_1+a_4)\Gamma(s_1+a_5)\Gamma(1-s_1)}{\Gamma(s_1+a_3)\Gamma(2-s_1)}\left(\frac{1}{a_2}\right)^{-s_1} \times \frac{1}{2\pi j}\int_{\mathcal{C}_2}\frac{\Gamma(s_2+\kappa_3)\Gamma(s_2)\Gamma(1-s_2)}{\Gamma(s_2+\frac{\xi^2}{r}+1)}\left(\frac{\mathcal{B}_1}{\kappa_{v_{D_r}}^2}\right)^{-s_2}\mathcal{I}_6(s_1)ds_1ds_2. \tag{107}$$

$$P_{b,1} \approx \frac{Ca_1\mathcal{Q}_1}{q^p}\sum_{m_1=1}^{\beta} b_{m_1} r^{\alpha+m_1-2}\sum_{k=0}^{\infty}\frac{(-1)^k}{k!}\left(C\kappa_{v_{D_r}}^2\right)^k\frac{1}{(2\pi j)^2}\int_{\mathcal{C}_1}\int_{\mathcal{C}_2}\mathcal{I}_1(s_1)\mathcal{I}_2(s_2)\Gamma(-s_2+s_1+1+k)ds_1ds_2 + \frac{a_1\mathcal{Q}_1}{q^p\kappa_{v_{D_r}}^2}\sum_{m_1=1}^{\beta} b_{m_1} r^{\alpha+m_1-2}\frac{1}{(2\pi j)^2}\int_{\mathcal{C}_1}\int_{\mathcal{C}_2}\mathcal{I}_3(s_1)\mathcal{I}_4(s_2)ds_1ds_2 \tag{109}$$

$$\mathcal{I}_4(s_2) = \frac{\Gamma(s_2+\frac{\varepsilon^2}{r})\prod_{\ell=0}^{r-1}\Gamma\left(s_2+\frac{\alpha+\ell}{r}\right)\prod_{\ell=0}^{r-1}\Gamma\left(s_2+\frac{m_1+\ell}{r}\right)\Gamma(s_2+1+m_I)\Gamma(s_2)\Gamma(1-s_2)}{\Gamma(s_2+\frac{\varepsilon^2}{r}+1)}\left(\frac{\mathcal{B}_1}{\kappa_{v_{D_r}}^2}\right)^{-s_2}. \tag{113}$$

REFERENCES

[1] C. Perera, A. Zaslavsky, P. Christen, and D. Georgakopoulos, "Context aware computing for the Internet of Things: A survey," *IEEE Commun. Surveys Tuts.*, vol. 16, no. 1, pp. 414–454, 1st Quart., 2014.

[2] M. Z. Chowdhury, M. K. Hasan, M. Shahjalal, M. T. Hossan, and Y. M. Jang, "Optical wireless hybrid networks: Trends, opportunities, challenges, and research directions," *IEEE Commun. Surveys Tuts.*, vol. 22, no. 2, pp. 930–966, 2nd Quart., 2020.

[3] E. Illi, F. E. Bouanani, K.-H. Park, F. Ayoub, and M.-S. Alouini, "An improved accurate solver for the time-dependent RTE in underwater optical wireless communications," *IEEE Access*, vol. 7, pp. 96478–96494, 2019.

[4] Z. Zeng, S. Fu, H. Zhang, Y. Dong, and J. Cheng, "A survey of underwater optical wireless communications," *IEEE Commun. Surveys Tuts.*, vol. 19, no. 1, pp. 204–238, 1st Quart., 2017.

[5] M. V. Jamali, P. Khorramshahi, A. Tashakori, A. Chizari, S. Shahsavari, S. AbdollahRamezani, M. Fazelian, S. Bahrani, and J. A. Salehi, "Statistical distribution of intensity fluctuations for underwater wireless optical channels in the presence of air bubbles," in *Proc. Iran Workshop Commun. Inf. Theory (IWCIT)*, May 2016, pp. 1–6.

[6] P. Combeau, S. Joumessi-Demeffo, A. Julien-Vergonjanne, L. Aveneau, S. Sahuguède, H. Boeglen, and D. Sauveron, "Optical wireless channel simulation for communications inside aircraft cockpits," *J. Lightw. Technol.*, vol. 38, no. 20, pp. 5635–5648, Oct. 15, 2020.

[7] A. Douik, H. Dahrouj, T. Y. Al-Naffouri, and M.-S. Alouini, "Hybrid radio/free-space optical design for next generation backhaul systems," *IEEE Trans. Commun.*, vol. 64, no. 6, pp. 2563–2577, Jun. 2016.

[8] Y. Chen, "Energy harvesting for wireless relaying systems," in *Wireless Information and Power Transfer: A New Paradigm for Green Communication*. Cham, Switzerland: Springer, 2018, pp. 123–155, doi: 10.1007/978-3-319-56669-6_5.

[9] H. Elahi, K. Munir, M. Eugeni, S. Atek, and P. Gaudenzi, "Energy harvesting towards self-powered IoT devices," *Energies*, vol. 13, no. 21, p. 5528, Oct. 2020. [Online]. Available: https://www.mdpi.com/1996-1073/13/21/5528

[10] M. J. Saber, J. Mazloum, A. M. Sazdar, A. Keshavarz, and M. J. Piran, "On secure mixed RF-FSO decode-and-forward relaying systems with energy harvesting," *IEEE Syst. J.*, vol. 14, no. 3, pp. 4402–4405, Sep. 2020.

[11] Y. Wang, Y. Tong, and Z. Zhan, "On secrecy performance of mixed RF-FSO systems with a wireless-powered friendly jammer," *IEEE Photon. J.*, vol. 14, no. 2, pp. 1–8, Apr. 2022.

[12] W. K. Harrison, J. Almeida, M. R. Bloch, S. W. McLaughlin, and J. Barros, "Coding for secrecy: An overview of error-control coding techniques for physical-layer security," *IEEE Signal Process. Mag.*, vol. 30, no. 5, pp. 41–50, Sep. 2013.

[13] M. Bloch and J. Barros, *Frontmatter*. Cambridge, U.K.: Cambridge Univ. Press, 2011, pp. 1–6.

[14] A. O. Hero, "Secure space-time communication," *IEEE Trans. Inf. Theory*, vol. 49, no. 12, pp. 3235–3249, Dec. 2003.

[15] A. D. Wyner, "The wire-tap channel," *Bell Syst. Tech. J.*, vol. 54, no. 8, pp. 1355–1387, Oct. 1975.

[16] E. Illi, "Performance evaluation of mixed RF-UOWC system with residual hardware impairments," in *Proc. 4th Int. Conf. Adv. Commun. Technol. Netw. (CommNet)*, Dec. 2021, pp. 1–7.

[17] E. Balti and B. K. Johnson, "On the joint effects of HPA nonlinearities and IQ imbalance on mixed RF/FSO cooperative systems," *IEEE Trans. Commun.*, vol. 69, no. 11, pp. 7879–7894, Nov. 2021.

[18] K. Guo, B. Zhang, Y. Huang, and D. Guo, "Performance analysis of a satellite–multi-terrestrial relay network with hardware impairments using switch-and-stay combining scheme," *Int. J. Distrib. Sensor Netw.*, vol. 13, no. 9, p. 11, 2017.

[19] E. Balti, M. Guizani, B. Hamdaoui, and B. Khalfi, "Aggregate hardware impairments over mixed RF/FSO relaying systems with outdated CSI," *IEEE Trans. Commun.*, vol. 66, no. 3, pp. 1110–1123, Mar. 2018.

[20] H. Wu, Y. Zou, W. Cao, Z. Chen, T. A. Tsiftsis, M. R. Bhatnagar, and R. C. De Lamare, "Impact of hardware impairments on outage performance of hybrid satellite-terrestrial relay systems," *IEEE Access*, vol. 7, pp. 35103–35112, 2019.

[21] J. Ding, D. Kang, X. Xie, L. Wang, L. Tan, and J. Ma, "Joint effects of co-channel interferences and pointing errors on dual-hop mixed RF/FSO fixed-gain and variable-gain relaying systems," *IEEE Photon. J.*, vol. 15, no. 1, pp. 1–11, Feb. 2023.

[22] M. N. Bashir, K. M. Yusof, and S. Iqbal, "Outage performance analysis of UAV-assisted dual-hop cooperative network under distortions and interferences," in *Proc. 8th Int. Conf. Inf. Technol. Trends (ITT)*, May 2022, pp. 45–50.

[23] E. Soleimani-Nasab and M. Uysal, "Generalized performance analysis of mixed RF/FSO cooperative systems," *IEEE Trans. Wireless Commun.*, vol. 15, no. 1, pp. 714–727, Jan. 2016.

[24] E. Balti and M. Guizani, "Mixed RF/FSO cooperative relaying systems with co-channel interference," *IEEE Trans. Commun.*, vol. 66, no. 9, pp. 4014–4027, Sep. 2018.

[25] S. Labghough, F. Ayoub, F. E. Bouanani, M. Belkasmi, and K. A. Qaraqe, "Mixed RF/FSO SWIPT-based OSLMD coded AF cooperative communication system: Performance analysis," *IEEE Trans. Green Commun. Netw.*, vol. 7, no. 1, pp. 84–100, Mar. 2023.

[26] S. Labghough, F. Ayoub, and M. Belkasmi, "Error probability analysis for dual-hop mixed RF-FSO system using CSOC codes with MLGD decoding," in *Proc. 15th Int. Wireless Commun. Mobile Comput. Conf. (IWCMC)*, Jun. 2019, pp. 378–383.

[27] S. Labghough, F. Ayoub, F. E. Bouanani, M. Belkasmi, and K. A. Qaraqe, "Performance analysis of polar codes over Fox's H-fading channels with RHI and IQI impairments," *IEEE Access*, vol. 11, pp. 22505–22512, 2023.

[28] A. Eslami, S. Vangala, and H. Pishro-Nik, "Hybrid channel codes for efficient FSO/RF communication systems," *IEEE Trans. Commun.*, vol. 58, no. 10, pp. 2926–2938, Oct. 2010.

[29] M. N. Khan and M. Jamil, "EXIT chart behaviour for the hybrid FSO/RF communication system," in *Proc. 10th Int. Conf. Inf., Commun. Signal Process. (ICICS)*, Dec. 2015, pp. 1–5.

[30] P. Chen, B. Bai, Z. Ren, J. Wang, and S. Sun, "Hash-polar codes with application to 5G," *IEEE Access*, vol. 7, pp. 12441–12455, 2019.

[31] H. Kashif, M. N. Khan, and Z. Nawaz, "Analysis of LDPC code in hybrid communication systems," *Comput., Mater. Continua*, vol. 74, no. 1, pp. 769–781, Jan. 2023. [Online]. Available: http://www.techscience.com/cmc/v74n1/49866

[32] S. A. H. Mohsan, M. A. Khan, and H. Amjad, "Hybrid FSO/RF networks: A review of practical constraints, applications and challenges," *Opt. Switching Netw.*, vol. 47, Feb. 2023, Art. no. 100697. [Online]. Available: https://www.sciencedirect.com/science/article/pii/S1573427722000339

[33] H. Kashif and M. N. Khan, "Outage probability analysis of free space communication system using diversity combining techniques," *Comput., Mater. Continua*, vol. 73, no. 3, pp. 6001–6017, 2022. [Online]. Available: http://www.techscience.com/cmc/v73n3/49087

[34] N. Vishwakarma and R. Swaminathan, "Performance analysis of hybrid FSO/RF communication over generalized fading models," *Opt. Commun.*, vol. 487, May 2021, Art. no. 126796. [Online]. Available: https://www.sciencedirect.com/science/article/pii/S0030401821000468

[35] X. Cui, D. Wang, C. Sun, H. Sun, and M. Zhang, "A flexible FPGA based QC-LDPC decoder for the adaptive coding and modulation scheme of broadband satellite communication system," in *Proc. IEEE 21st Int. Conf. Commun. Technol. (ICCT)*, Oct. 2021, pp. 1368–1371.

[36] F. El Bouanani and D. B. D. Costa, "Accurate closed-form approximations for the sum of correlated Weibull random variables," *IEEE Wireless Commun. Lett.*, vol. 7, no. 4, pp. 498–501, Aug. 2018.

[37] E. Illi, F. E. Bouanani, and F. Ayoub, "Physical layer security of an amplify-and-forward energy harvesting-based mixed RF/UOW system," in *Proc. Int. Conf. Adv. Commun. Technol. Netw. (CommNet)*, 2019, pp. 1–8.

[38] I. S. Gradshteyn and I. M. Ryzhik, *Table of Integrals, Series, and Products*. Burlington, MA, USA: Elsevier, 2007.

[39] A. A. Farid and S. Hranilovic, "Outage capacity optimization for free-space optical links with pointing errors," *J. Lightw. Technol.*, vol. 25, no. 7, pp. 1702–1710, Jul. 2007.

[40] E. Illi, F. E. Bouanani, and F. Ayoub, "A performance study of a hybrid 5G RF/FSO transmission system," in *Proc. Int. Conf. Wireless Netw. Mobile Commun. (WINCOM)*, Nov. 2017, pp. 1–7.

[41] E. Lee, J. Park, D. Han, and G. Yoon, "Performance analysis of the asymmetric dual-hop relay transmission with mixed RF/FSO links," *IEEE Photon. Technol. Lett.*, vol. 23, no. 21, pp. 1642–1644, Nov. 1, 2011.

[42] I. S. Ansari, "On the performance of free-space optical systems over generalized atmospheric turbulence channels with pointing errors," Ph.D. dissertation, Division Comput., Elect., Math. Sci. Eng., King Abdullah Univ. Sci. Technol. (KAUST), Thuwal, Saudi Arabia, Feb. 2015.

[43] S. Lin and D. J. Costello, *Error Control Coding: Fundamentals and Applications*. Englewood Cliffs, NJ, US: Pearson, 1983.

[44] W. Wu, "New convolutional codes—Part I," *IEEE Trans. Commun.*, vol. COM-23, no. 9, pp. 942–956, Sep. 1975.

[45] J. L. Massey, "Threshold decoding," Ph.D. dissertation, Massachusetts Inst. Technol., Cambridge, MA, USA, Apr. 1963.

[46] W. Wu, "New convolutional codes—Part II," *IEEE Trans. Commun.*, vol. COM-24, no. 1, pp. 19–33, Jan. 1976.

[47] *Mathematica, Version 13.2*, Wolfram, Champaign, IL, USA, 2022. [Online]. Available: https://functions.wolfram.com

[48] A. Goldsmith, *Wireless Communications*. Cambridge, U.K.: Cambridge Univ. Press, 2005.

[49] G. C. Clark and J. B. Cain, *Error-Correction Coding for Digital Communications*. Boston, MA, USA: Springer, 1981.

[50] M. D. Springer, *The Algebra of Random Variables* (Probability and Mathematical Statistics). New York, NY, USA: Wiley, 1979.

[51] A. A. Kilbas, *H-Transforms: Theory and Applications*. Boston, MA, USA: Springer, 2004.

[52] A. Kilbas and M. Saigo, *H-Transforms: Theory and Applications*. Boston, MA, USA: Springer, Mar. 2004.

[53] T. N. Srivastava, "Certain properties of bivariate distributions involving the H-function of Fox," *Can. J. Statist.*, vol. 4, no. 2, pp. 227–236, 1976. [Online]. Available: http://www.jstor.org/stable/3315138

SOUAD LABGHOUGH was born in Rabat, Morocco, in July 1992. She received the B.Sc. and M.Sc. degrees in computer sciences, telecommunications, and electrical engineering from Mohammed V University in Rabat, Morocco, in 2013 and 2015, respectively, where she is currently pursuing the Ph.D. degree with the Information, Communication and Embedded Systems (ICES) Team, ENSIAS Engineering School. In 2021, she was a Research Assistant with Texas A&M University at Qatar. Her current research interests include error-correcting codes, information theory, free space optical communication, and channel modeling in 5G WCSs.

FOUAD AYOUB (Member, IEEE) was born in Kenitra, Morocco, in 1979. He received the B.Sc. degree in applied physics and the M.Sc. and Ph.D. degrees in engineering, telecommunications, and multimedia from the Faculty of Sciences, Mohammed V University at Rabat, Morocco, in 2002, 2005, and 2011, respectively. From 2012 to 2016, he was an Assistant Professor with CRMEF, Morocco, where he is currently an Associate Professor. He advised the master's and Ph.D. students at both Mohammed V University at Rabat and Ibn Tofail University. So far, his research efforts have culminated papers in a wide variety of international conferences and journals, including the IEEE Transactions on Vehicular Technology, IEEE Access, the IEEE Transactions on Sustainable Computing, IWCMC, CommNet, and Globecom. His current research interests include telecommunications, information and coding theory, and the performance analysis of WCSs. He was the General Co-Chair of the 2019 CommNet Conference and the 2020 CommNet Conference and the General Chair of the 2018 ICSDE Workshop and the Chair Registration and Publications of the 2016 ACOSIS Conference and the 2018 CommNet Conference. He has served as a reviewer for many international journals.

FAISSAL EL BOUANANI (Senior Member, IEEE) was born in Nador, Morocco, in 1974. He received the M.S. and Ph.D. degrees in network and communication engineering from Mohammed V University–Souissi, Rabat, Morocco, in 2004 and 2009, respectively. He was a Faculty Member with the University of Moulay Ismail, Meknes, from 1997 to 2009. In 2009, he joined the National High School, IT/ENSIAS College of Engineering, Mohammed V University at Rabat, in 2009, where he is currently an Associate Professor. He advised many master's and Ph.D. students with Mohammed V University at Rabat and the University of Moulay Ismail. So far, his research efforts have culminated in more than 110 papers in a wide variety of IEEE/ACM international conferences and journals. His current research interests include performance analysis and design of WCSs. He has been involved as a TPC member in various conferences and IEEE journals. His Ph.D. thesis was awarded the best one by Mohammed V University–Souissi, in 2010. He served as the TPC Chair for the ICSDE Conference and the General Co-Chair for the ACOSIS 2016 Conference and the 2017–2023 CommNet Conference. He served as the TPC Chair for the ICSDE Conference and the General Chair for the CommNet Conferences. He is currently an Associate Editor of IEEE Access and *Frontiers in Communications and Networks* journal. He is also serving as a Lead Guest Editor for the Special Issues on Physical Layer Security of *Frontiers in Communications and Networks* journal.

MOSTAFA BELKASMI (Member, IEEE) received the Ph.D. degree from Toulouse III University, Toulouse, France, in 1992. He is currently a Professor with the ENSIAS College of Engineering and the Head of the Information, Communication and Embedded Systems (ICES) Team, Mohammed V University at Rabat, Morocco. His research has so far resulted in papers that have been published in numerous international conferences and journals. His current research interests include mobile and WCSs, channel coding, and cybersecurity. He served as the General Chair of the 2016 and 2019 Editions of the ACOSIS Conference and of the 2014 Edition of the AfricaCrypt Conference. He has reviewed articles for a variety of international journals.

KHALID A. QARAQE (Senior Member, IEEE) was born in Bethlehem. He received the B.S. degree (Hons.) in electrical engineering from the University of Technology, Bagdad, Iraq, in 1986, the M.S. degree in electrical engineering from The University of Jordan, Amman, Jordan, in 1989, and the Ph.D. degree in electrical engineering from Texas A&M University, College Station, TX, USA, in 1997. From 1989 to 2004, he has held a variety positions in many companies and has more than 12 years of experience in the telecommunication industry. He joined the Department of Electrical and Computer Engineering, Texas A&M University at Qatar, Qatar, in July 2004, where he is currently a Professor and the Managing Director of the Center for Remote Healthcare Technology, Qatar. He has worked on numerous projects and has experience in product development, design, deployments, testing, and integration. He has been awarded more than 20 research projects consisting of more than USD 13M from local industries in Qatar and the Qatar National Research Foundation (QNRF). He has published more than 131 journal articles in top IEEE journals and has published and presented 250 papers at prestigious international conferences. He has 20 book chapters published, four books, three patents, and presented several tutorials and talks. His current research interests include communication theory and its application to design and performance, analysis of cellular systems, indoor communication systems, mobile networks, broadband wireless access, cooperative networks, cognitive radio, diversity techniques, index modulation, visible light communication, FSO, tele-health, and noninvasive bio sensors.